Infectious Agents and Cancer

REVIEW   **Open Access**

Diagnostic evaluation and ablation treatments assessment in hepatocellular carcinoma

Vincenza Granata[1], Roberta Grassi[2,3], Roberta Fusco[4*], Andrea Belli[5], Carmen Cutolo[6], Silvia Pradella[7], Giulia Grazzini[7], Michelearcangelo La Porta[8], Maria Chiara Brunese[9], Federica De Muzio[9], Alessandro Ottaiano[10], Antonio Avallone[10], Francesco Izzo[5] and Antonella Petrillo[1]

Abstract

This article provides an overview of diagnostic evaluation and ablation treatment assessment in Hepatocellular Carcinoma (HCC). Only studies, in the English language from January 2010 to January 202, evaluating the diagnostic tools and assessment of ablative therapies in HCC patients were included. We found 173 clinical studies that satisfied the inclusion criteria.

HCC may be noninvasively diagnosed by imaging findings. Multiphase contrast-enhanced imaging is necessary to assess HCC. Intravenous extracellular contrast agents are used for CT, while the agents used for MRI may be extracellular or hepatobiliary. Both gadoxetate disodium and gadobenate dimeglumine may be used in hepatobiliary phase imaging. For treatment-naive patients undergoing CT, unenhanced imaging is optional; however, it is required in the post treatment setting for CT and all MRI studies. Late arterial phase is strongly preferred over early arterial phase. The choice of modality (CT, US/CEUS or MRI) and MRI contrast agent (extracelllar or hepatobiliary) depends on patient, institutional, and regional factors. MRI allows to link morfological and functional data in the HCC evaluation. Also, Radiomics is an emerging field in the assessment of HCC patients. Postablation imaging is necessary to assess the treatment results, to monitor evolution of the ablated tissue over time, and to evaluate for complications. Post- thermal treatments, imaging should be performed at regularly scheduled intervals to assess treatment response and to evaluate for new lesions and potential complications.

Keywords: HCC, Ultrasound, Computed tomography;magnetic resonance imaging, Radiomics, Ablation treatment assessment

Introduction

Primary liver cancer is the sixth most commonly diagnosed cancer and the third leading cause of cancer death worldwide in 2020, with approximately 906,000 new cases and 830,000 deaths. Rates of both incidence and mortality are 2 to 3 times higher among men than among women in most regions, and liver cancer ranks fifth in terms of global incidence and second in terms of mortality for men. Incidence rates among men are 2.4-fold greater in transitioned countries, but the highest rates are observed mainly in transitioning countries, with the disease being the most common cancer in 11 geographically *differents* countries in Eastern Asia, South-Eastern Asia, and Northern and Western Africa [1, 2].

Primary liver cancer includes hepatocellular carcinoma (HCC) (comprising 75–85% of cases) and intrahepatic cholangiocarcinoma (10–15%), as well as other rare types. The main risk factors for HCC are chronic infection with hepatitis B virus (HBV) or hepatitis C virus

* Correspondence: r.fusco@igeamedical.com
[4]Medical Oncology Division, Igea SpA, Naples, Italy
Full list of author information is available at the end of the article

Granata *et al. Infectious Agents and Cancer*   (2021) 16:53

Page 2 of 22

(HCV), aflatoxin-contaminated foods, heavy alcohol intake, excess body weight, type 2 diabetes, and smoking [1]. The major risk factors appear to be in transition, with the prevalence of HBV and HCV declining and excess body weight and diabetes increasing in many regions [1]. Although the relevance of nonviral risk factors is becoming more important, the elimination of viral hepatitis remains the key strategy for primary prevention of liver cancer globally, seeing as HBV infection and HCV infection account for 56 and 20% of liver cancer deaths worldwide, respectively [1, 2].

Patients who are diagnosed at an early stage without metastasis are eligible for curative treatments, and hence, have a good prognosis in the range of 50–70% survival rate at 5-year [3–8]. However, the prognosis is poor when HCC is diagnosed at an advanced stage. Therefore, an early detection of HCC and an accurate characterization of focal liver nodule on patient at risk for HCC is mandatory for a suitable patient management [5].

Nowadays, the gold standard for HCC diagnosis is the needle biopsy, but this is an invasive and dangerous technique. The non-invasive criteria for HCC diagnosis are based on the presence of the specific vascular profile on imaging assessment, characterized by contrast uptake during arterial phase, defined as arterial hyperenhancement, and followed by washout in the venous/portal phase [9–12]. However, arterial hyperenhancement and wash out appearance have a sensitivity rate of 50–60% in lesion smaller than 2 cm [9]. Therefore, other functional parameters have been introduced in the detection and characterization of HCC nodules [9–13]. Diffusion Weighted Imaging (DWI) has been applied to liver imaging as an excellent tool for detection and characterization of focal liver lesions, increasing clinical confidence and decreasing false positives [13].

Tumor ablation is a minimally invasive approach that is commonly employed in the treatment of hepatic tumors [14]. Ablation therapy is considered a potential first-line treatment in many patients with small hepatocellular carcinomas (< 3 cm) [15] or an alternative for people who are not fit for surgical resection [16, 17]. Moreover, tumor ablation can also be useful as an adjuvant therapy or may provide an alternative strategy to surgery or be used in association with resection in case of patients unfit for surgical treatments [17–21]. Ablation therapies, as stand alone or in combination, have created a new challenge for radiologists, who should assess the response. The goal of locoregional therapy is inducing necrosis. Therefore, tumor shrinkage may not be apparent or may be absent with thermal approaches. Tumor physiologic features such as angiogenesis and hypoxia are more relevant to demonstrating tumor response in this setting, and thus require the development of new functional imaging biomarkers.

Our aim is to report an overview and update on diagnostic assessment in HCC patients.

Methods
This narrative review is the result of autonomous study without protocol and registration number.

Search criterion
Several electronic datasets were searched: PubMed (US National Library of Medicine, http://www.ncbi.nlm.nih.gov/pubmed), Scopus (Elsevier, http://www.scopus.com/), Web of Science (Thomson Reuters, http://apps.webofknowledge.com/) and Google Scholar (https://scholar.google.it/). The following search criteria have been used: "HCC" AND "Ultrasound", "HCC" AND "Computed Tomography", "HCC" AND "Magnetic Resonance Imaging", "HCC" AND "Radiomics", "HCC" AND "Li-RADS", "HCC" AND "Ablative Therapies" AND "Assessment".

The search covered the years from January 2010 to April 2021. Moreover, the reference lists of the found papers were analysed for papers not indexed in the electronic databases. All titles and abstracts were analysed. The inclusion criteria were clinical study (eg. retrospective analysis, case series, prospective cohort study) evaluating the diagnostic tools and safety and efficacy of ablative therapies in HCC patients. Articles published in the English language from January 2010 to January 2021 were included. Exclusion criteria were different topics, unavailability of full text, not sufficient data and case report, review, or letter to editors.

Results
We identified 4220 potentially relevant references through electronic searches. After removing 2809 duplicates, we obtained 1411 references. We identified 25 references through scanning reference lists of the identified randomized trials that we added to the 1411 references previously selected (total number of scrutinized articles was 1436). We then excluded 1098 clearly irrelevant articles through screening titles and reading abstracts. We excluded 165 references for the reasons listed in the exclusion criteria. A total of 173 clinical trials met the inclusion criteria. The reference flow is summarized in the study flow diagram (Fig. 1).

Discussion
Diagnostic tools
Ultrasound
Ultrasound (US) is an imaging tool is cheap, non-invasive, non-irradiating and, thus, repeatable, suitable for patient disease monitoring [22–25]. Contrast-

Fig. 1 Included and excluded studies in systematic review
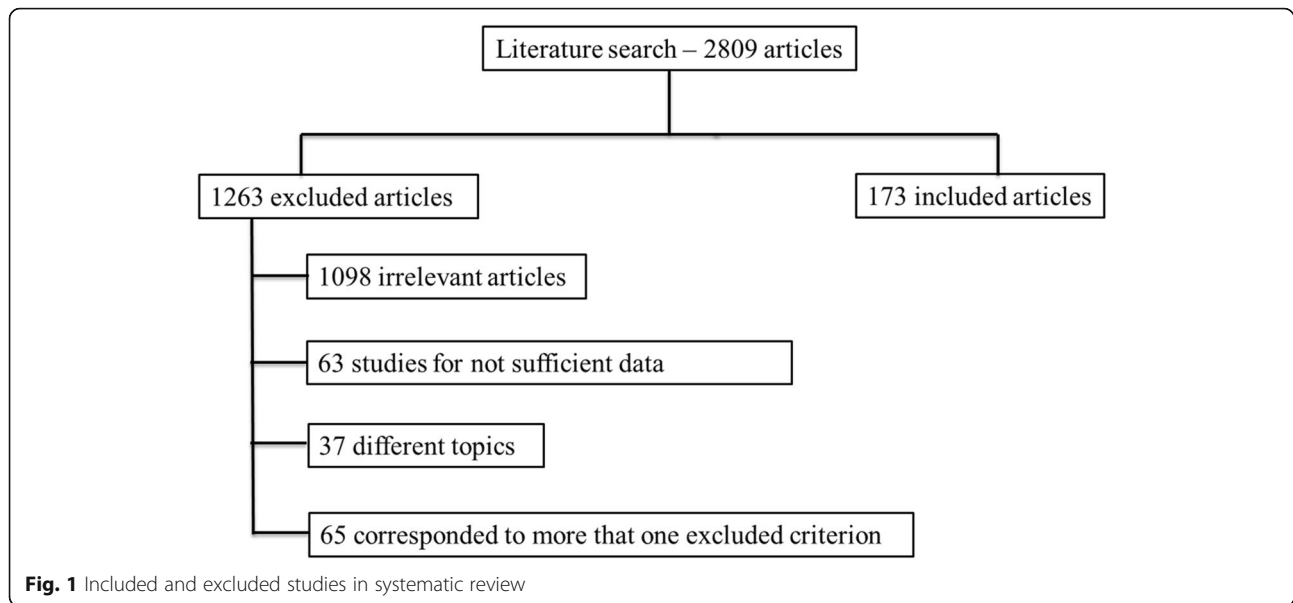
Enhanced Ultrasound (CEUS) imaging is an improved ultrasound-based technology, assuming the injection into the blood of a specific contrast agent, consisting of gas filled microbubbles [22]. The contrast agent spreads through the human body, emphasizing the vessel structure in the region of interest [22]. This technology leads to the highlighting of both large vessel flows, as well as of the microcirculation, being firstly implemented for hepatic tumor pathology, for abdominal emergencies and in order to recognize various tumor types [26–36]. The microbubbles of the contrast agent produce harmonic echoes, which are detected by the transducer. This behavior is significantly different from that of the usual US waves reflected by the tissues [22].

Within B-mode US images, HCC appears, in more advanced evolution phases, as a well-defined region, of 3–5 cm in size, being hyperechogenic and often heterogeneous, due to the interleaving of fatty cells, necrosis, fibrosis and active growth tissue (Fig. 2) [22]. In CEUS images, HCC appears more highlighted, due to the dense

and complex vessel structure that is specific to the malignant tumors (Fig. 3) [22]. The HCC tumors are usually hyperenhanced during the arterial phase, showing washout during the portal venous and delayed phases (Fig. 4) [22].

However, in many cases, within both B-mode US images and CEUS images, HCC is hardly distinguishable from the cirrhotic parenchyma.

Computed tomography

Currently, contrast-enhanced computed tomography (CE-CT) is commonly used for the noninvasive detection and characterization of focal liver lesions (FLLs) due to its high scanning speed and high-density resolution [37–47]. The appearances, especially the dynamic enhancement patterns of FLLs on CT imaging, are essential for categorizing lesions. With the careful evaluation of CT images, for most liver lesions the diagnosis can be achieved with a relatively high accuracy [37]. However, in current clinical practice, the evaluation of
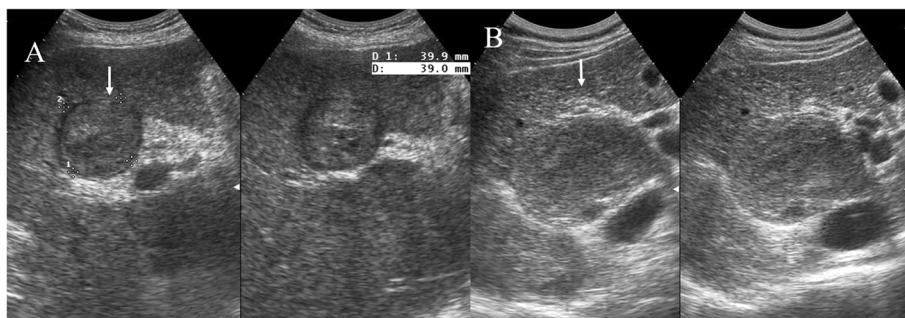

Fig. 2 US assessment of HCC on IV a hepatic segment. The lesion (arrow) is hyper-isoechoic compared to liver parenchyma
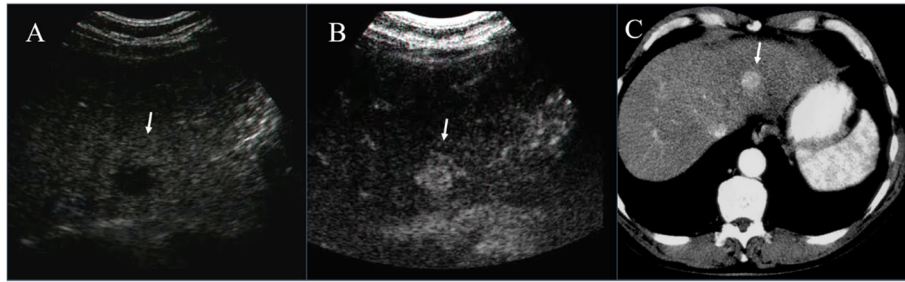
Fig. 3 US (**A**), CEUS (**B**) and CT (**C**) assessment of HCC on II hepatic segment. The lesion in **B** and **C** (arrow) shows hyperenhancement during arterial phase of contrast study

CT images is mainly performed by radiologists. The results are influenced by the radiologist's experience and are generally subjective [37].

Multiphase contrast-enhanced computed tomography (CT) is often the first diagnostic imaging technique to diagnose HCC, and besides, Magnetic Resonance Imaging (MRI) represents the standard imaging method. For daily clinical routine, CT is the best available technique, and in contrast to CEUS it is examiner-independent [48]. Thus, CT allows a fast, reproducible and non very expensive examination. Especially for patients with reduced general state of health and restricted compliance, CT offers an adequate examination in contrast to MRI or CEUS, which are more dependent on the compliance of the patient [48].

Classical CT protocol in the assessment of HCC involves multiphase study with non-contrast phase, arterial, portal/venous, and equilibrium phase [49]. The non-contrast phase is useful to detect hyperattenuation due to haemorrhage or hyperattenuating embolic agents like lipiodol before contrast administration, thus avoiding misinterpretation of arterial-phase hyperenhancement [49]. The arterial phase, which is characterized by full enhancement of the hepatic artery and beginning enhancement of the portal vein, is useful to detect hypervascular HCC [49]. The portal venous phase which is

characterized by enhancement of hepatic veins as well as portal veins and the equilibrium phase imaging are useful for the differential diagnosis of HCC. Infact, the majority of HCCs shows washout of contrast medium in these phases (Figs. 5 and 6) [49]. However, early HCCs and dysplastic nodules are often iso- or hypo-vascularized with different enhancement patterns compared to hypervascularized advanced HCCs [49]. Early HCC can show iso-attenuation throughout all phases of dynamic CT (Fig. 7) [49].

Newer techniques have been introduced to increase lesion detection and characterization, such as dual-energy CT (DECT) with low-energy acquisition at 80 kVp instead of the frequently applied 120 kVp [45, 50–59]. DECT, which is based on simultaneously acquisition of two datasets at different energy levels, has the potential to generate virtual monochromatic images (VMIs). These images have higher contrast at lower energy levels because they use an approximation of energy levels closer to the k-edge of iodine at 33 keV [59]. Yoon et al. showed that low monoenergetic images (50 keV) allowed significantly better focal liver lesion conspicuity even after lowering both radiation and contrast media doses by 30%, compared with standard-dose in non obese patients [58]. Furthermore, 50 keV images obtained using the double low-dose CT protocol revealed higher image
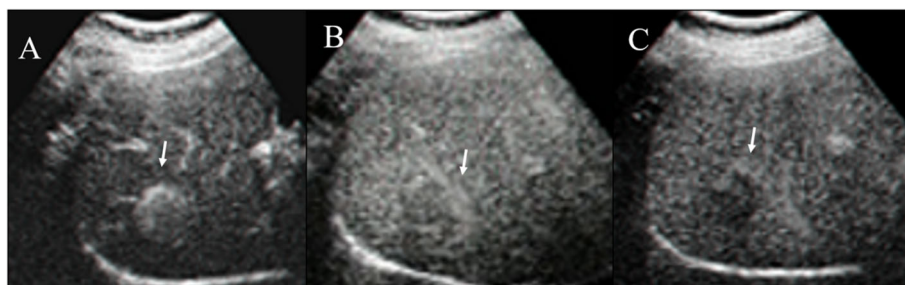

Fig. 4 Ceus evaluation of HCC on VIII liver segment. During contrast study, the lesion (arrow) shows hyperenhancement during arterial phase (**A**), wash out during portal (**B**) and equilibrium (**C**) phase
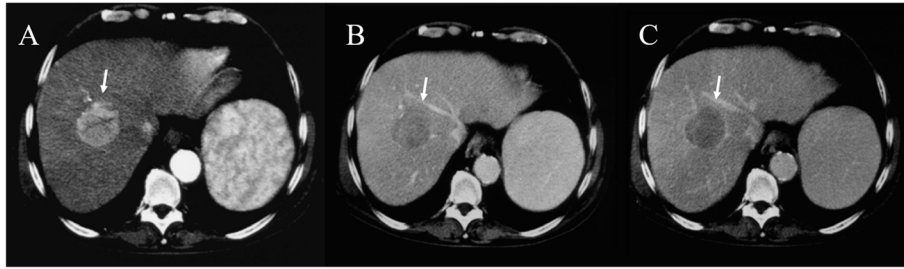
Fig. 5 The same case of Fig. 4. CT assessment. During contrast study, the lesion (arrow) shows hyperenhancement during arterial phase (**A**), wash out during portal (**B**) and equilibrium (**C**) phase

contrast, and better image quality than standard-dose iDose images at both arterial and portal venous phases [58]. Simultaneous radiation and contrast media dose reduction would particularly be useful for patients who undergo multiple CT scans. Patients with a suspicion of HCC or a history of HCC belong to this category owing to the demand for an intense follow-up strategy due to the high risk of HCC recurrence. However, radiation exposure is often underestimated in oncologic patients due to their relatively short life expectancy and the clinicians' focus on the immense benefit of early detection of recurrence [58–61]. Indeed, patients with very early or early-stage HCCs who have a life expectancy of longer than 5 years, usually undergo multiple CT scans at 3- to 4-month intervals so as to detect recurrence [62]. Contrast media dose reduction should also be important for those patients because renal dysfunction is common in oncologic patients and cirrhotic patients [63]. Therefore, as suggested by Yoon, the reduction of radiation and contrast doses using DECT while maintaining image quality and diagnostic performance would hold great clinical value for patients with a high risk of HCCs who need to undergo multiple multiphasic liver CT scans [58].

Perfusion CT (pCT) is a non-invasive imaging tool based on contrast kinetics of tissue that supplies quantitative information on tissue hemodynamics. pCT measures dynamic changes in tissue iodine concentration over time, allowing for calculation of tissue-specific parameters, including blood flow (BF), blood volume (BV), time to peak concentration (TTP), vascular permeability surface area product (PS), and permeability (Ktrans), which can be used as surrogates for tumor vascularization, vascular immaturity, and perfusion pressure. Several researchers reported that pCT is argued to be a significant method for differentiating benign from malignant lesions, evaluating treatment response, and defining angiogenesis [64–66].

During the development of HCC from a low-grade dysplastic nodule to advanced HCC, the arterial blood supply and angiogenesis are increased. Quantifying HCC vascularity is important for evaluating tumor progression. pCT is highly promising as a functional vascular
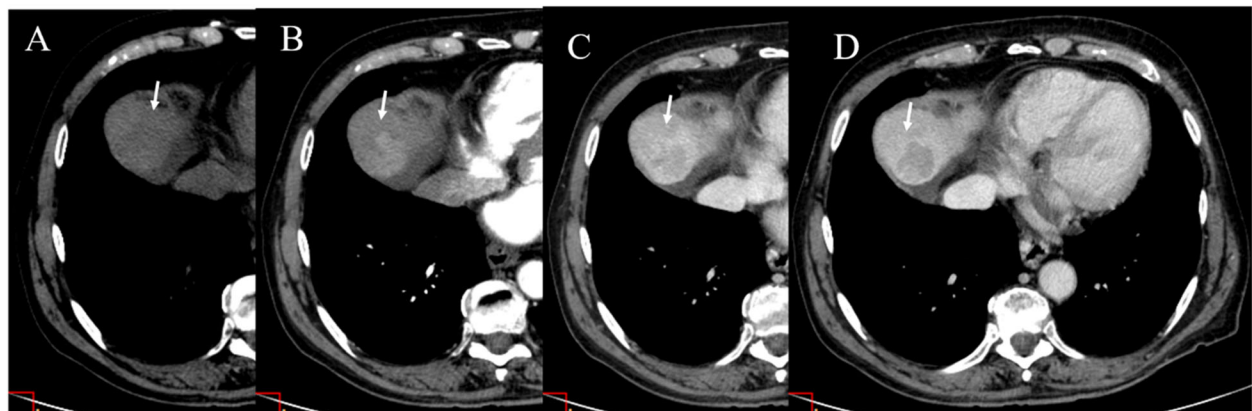
Fig. 6 CT assessment of HCC on IVa hepatic segment. In (**A**) pre contrast phase. During contrast study, the lesion (arrow) shows hyperenhancement during arterial phase (**B**), wash out during portal (**C**) and capsule appearance in equilibrium phase (**D**)

Granata *et al. Infectious Agents and Cancer* (2021) 16:53

Page 6 of 22
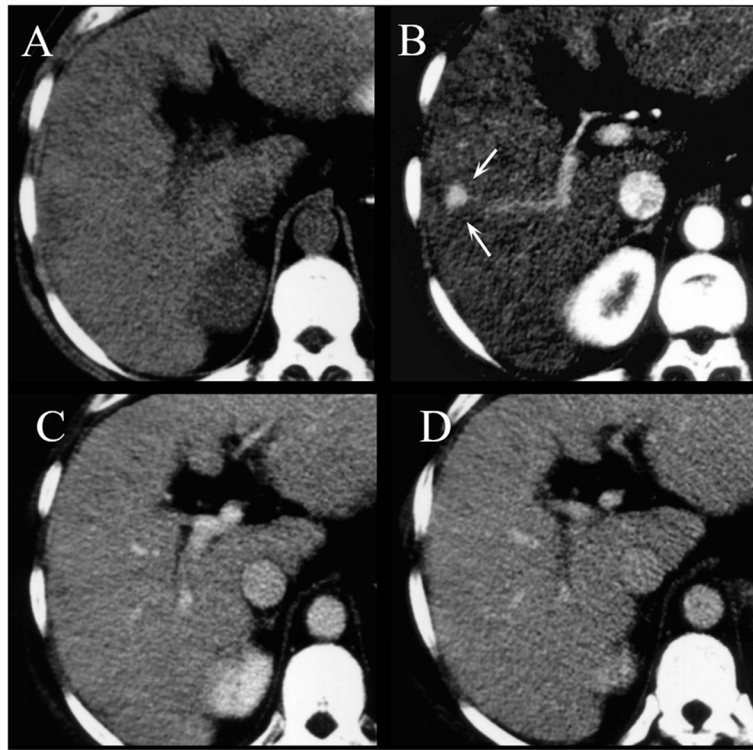
Fig. 7 Early HCC on V hepatic segment: pre contrast phase (**A**), arterial phase (**B**), portal phase (**C**), equilibrium phase (**D**). The lesion (arrows) is deteced only during arterial phase of contrast study (**B**)
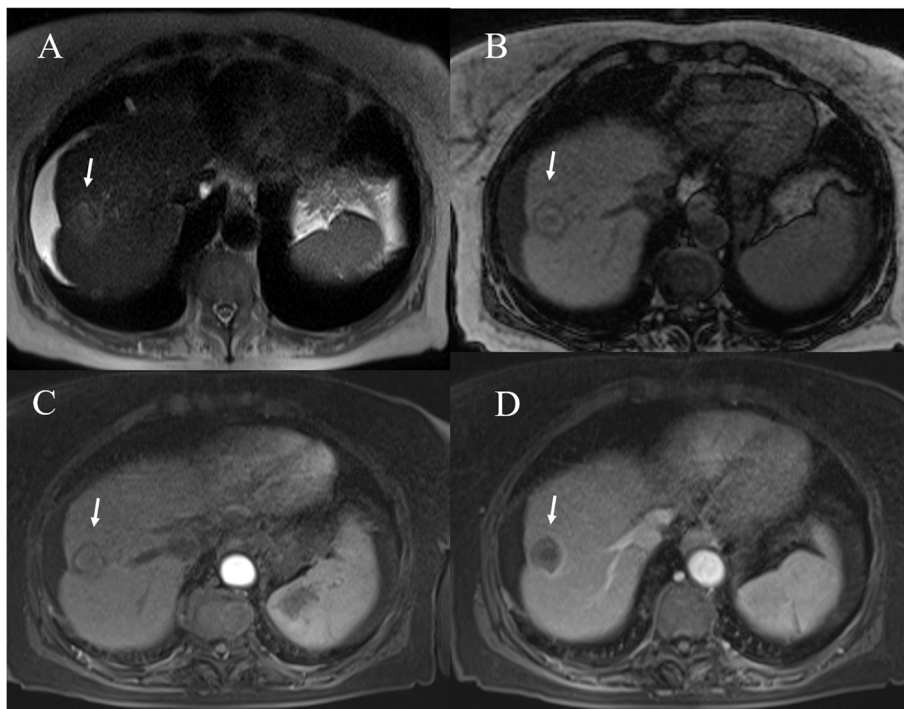
Fig. 8 MRI assessment of HCC on II hepatic segment. The lesion show (arrow) hyperintense signal in T2-W sequence (**A**), hyperehancement during arterial phase (**B**), wash out appearance (**C**) during portal phase and nodule in nodule appearance in hepatobiliary phase (**D**)

Granata *et al. Infectious Agents and Cancer* (2021) 16:53

Page 7 of 22

imaging technique. However, because of the increased radiation dose, CT perfusion of liver is largely unfulfilled clinically [64].

Magnetic resonance imaging

MRI is the imaging technique of choice in the assessment of focal liver lesions [67–73], particulary, in the diagnostic phase and during the follow up after treatment in HCC patients [74–82]. In the following section we will focus on several particular MRI features in the workup of HCC patients: morfological assessment, dynamic contrast enhancement (DCE)-MRI, diffusion-weighted imaging (DWI), Bold sequences.

Morfological assessment

MR imaging diagnosis of HCC is mainly based on assessment of vascularity, capsule appearance, and signal intensity (SI) during the hepatobiliary (EOB) phase. MR imaging also allows the assessment of morfological or ancillary features, that can be divided into those that favor the diagnosis of HCC specifically (intralesional fat, nodule-in-nodule architecture (Fig. 8), and mosaic architecture) and those that favor the diagnosis of malignancy but are not specific for HCC (mild-moderate T2 hyperintensity and lesional iron sparing) [9].

Intralesional fat is the presence of lipid within the nodule in higher concentration than in the hepatic parenchyma [9]. This feature can be detected at MR by observing signal loss in out-of-phase compared with inphaseT1-W GRE images. In a patient at risk for HCC, the detection of intralesional fat in a solid nodule raises concern for malignancy or premalignancy. In fact, this feature does not establish the diagnosis of HCC, however, as the differential diagnosis includes high-grade dysplastic nodule and occasionally low-grade dysplastic nodule [9].

Mosaic architecture refers to the presence within a mass of randomly distributed internal nodules differing in enhancement, intensity, often separated by fibrous septa. This feature is characteristic of large HCCs and reflects the mosaic configuration observed at pathologic evaluation. It is unusual in tumors other than HCC [9].

T2-W hyperintensity is an ancillary imaging features. Park et al. showed that dysplastic nodules and HCCs cannot be distinguished on the basis of signal intensity characteristics on unenhanced MRI, since their signal intensities are similar on T1- and T2-W sequences [83]. However, dysplastic nodules are almost never hyperintense on T2-W, early HCCs are mostly isointense on T2-W, while higher grade (moderately or poorly) of HCC is associated with high SI on T2-W images, although the SI may also be related with tumor vascularity and peliotic changes [83]. Previous study demonstrated that T2-W hyperintensity was a highly specific marker

of nodule malignancy, although poorly sensitive [84–87]. Golfieri et al. [87] showed that, compared to hypointensy on EOB phase, T2-W hyperintensity was a poor predictor of malignancy in the early stages of HCC. Conversely to Golfieri [87], Ouedraogo et al. [88] demonstrated that the addition of T2-W hyperintensity to the AASLD criteria increased the detection rate of HCC, especially for nodules smaller than 20 mm. In fact the sensitivity of MRI increased from 67.6 to 79%. Hwang et al. [89] compared the diagnostic performance of DWI and T2-W images in differentiating between hypovascular HCC and dysplastic nodules seen as hypointense nodules at hepatobiliary phase. They showed that hyperintensity on T2-W and DWI were significant features for differentiating hypovascular HCCs from dysplastic nodules. Kim et al. [90] evaluated the most predictive finding among hyperintensity on T2-W, DWI, washout, capsular enhancement, and hypointensity on gadoxetic acid-enhanced hepatobiliary phase images in the detailed characterization of arterial phase enhancing nodules 1 cm in diameter and smaller. They showed that for hypervascular lesions of 1 cm in diameter or smaller, T2-weighted images have the highest sensitivity among tests with an odds ratio statistically separable from 1 for differentiating HCC from benign hypervascular lesions 1 cm or smaller.

Lesional iron sparing refers to relative paucity of iron in a solid mass compared with that of background iron overloaded liver. This feature raises concern for premalignancy or malignancy because high-grade dysplastic nodules and HCCs characteristically are iron "resistant". However it is not specific for high-grade dysplastic nodule or HCC, but other non-HCC malignancies may have this appearance [9].

Dynamic contrast-enhanced (DCE)-MRI

DCE-MRI provides functional parameters on tumour perfusion, vessel permeability and ex- tracellular-extravascular space composition by assessing the changes in SI after the injection of a paramagnetic contrast medium. DCE- MRI may estimate data of the tumour vascular microenvironment, such as hypoxia and microvascular density, and also vascular changes induced by treatments. DCE-MRI can be evaluated by qualitatively, semi quantitatively and quantitatively method. Quantitative analysis involves the assessment of the pharmacokinetics of an administered contrast medium [91–95]. The most commonly used feature is the volume transfer constant, Ktrans, which represents the rate of contrast medium that moves from the blood to the extracellular space and relates to microvascular blood flow, vessel wall permeability, and vessel density. Ktrans has been shown to be correlated with tumor vascular endothelial growth factor and tumor

Granata *et al. Infectious Agents and Cancer*   (2021) 16:53

Page 8 of 22

aggressiveness. However, being influenced by many variables and since many different models are present in the literature, the quantitative approach still suffers from high output variability, poor clinical consistency and reproducibility. Qualitative DCE-MRI (qMRI) analyzes the time–intensity curve (TIC), involving the visual inspection and classification of TIC. The main weakness of qMRI is the ROI positioning that makes this approach operator dependent. Semi-quantitativeDCE-MRI is based on the analysis of TIC shape descriptors providing immediate data, related to the pathophysiology of the tumour. This approach could be more robust in clinical practice compared to quantitative o qualitative method, since many critical issues are reduced. However, semi-quantitative parameters do not show a direct analysis of physiological appearance [96, 97].

Quantitative DCE-MR parameters are derived from a pharmacokinetic model analysis and, on the basis of the mathematical model used, they reflect the underlying perfusion and/or permeability of the target tissue. *K*trans can have different physiologic interpretations depending on the balance between the blood flow and capillary permeability in the target tissue. If the contrast material uptake is flow limited, then *K*trans is related to the tissue perfusion [97]. Theoretically, hypervascular tumors are usually composed of a larger vascular space (vp) relative to the interstitial space (ve) and show a pattern of rapid arterial enhancement followed by washout, whereas a hypovascular tumor usually consists of a larger ve relative to the vp and shows progressive enhancement [97]. The liver is a dual-blood-supply organ that accepts blood from both the hepatic artery and portal vein. This unique physiological structure means that calculating the quantitative DCE-MRI parameters differs from that for organs with a single blood supply. Based on the characteristics of the dual blood supply, most quantitative analysis of DCE-MRI of the liver is currently carried out using the dual-inputtwo-compartment extended Tofts (DITET) model [98–100]. However, given that HCCs are mainly supplied by the hepatic artery, the relative benefits of the single-inputtwo-compartment extended Tofts (SITET) and DITET models remain unclear [100]. However, although the arterial blood supply is relatively increased in HCC compared with the portal blood supply, the tumor still has a dual blood supply. Several researches showed that compared with the SITET model, both the permeability and perfusion parameters of DITE T correlated better with CD31- MVD and CD34-MVD, suggesting that the mathematical DITET model was more consistent with the microcirculation environment of HCC [100]. The permeability and perfusion parameters of the DITET model may thus be used to predict and evaluate the efficacy of targeted therapy and the response to transarterial chemoembolization in HCC, and

for the diagnosis and classification of hepatic fibrosis and evaluation of liver function [100].

Ktrans is an important pharmacokinetic parameter to assess vascular permeability and therapeutic effects after non-surgical treatment in HCC. Several studies have suggested that a larger drop of Ktrans is correlated with favorable clinical outcomes after sunitinib or Floxuridine therapy [101, 102]. However, the most important role of quantitative DCE-MRI is the assessment of treatment efficacy in advanced HCC after ablative methods. These treatments may not produce a change in Ktrans because Fp and PS may change in opposite directions. On the other hand, Fp and PS may be changed in varying proportions. In these types of situations, it is important to understand which part of the vasculature is affected by the treatment [103].

Diffusion weighted imaging-MRI

DWI offers functional quantitative data on the tissue's microstructure by means of the water proton mobility differences and cellular density evaluation. Water diffusion mobility is linked to cell density, vascularity and viscosity of the extracellular apparent diffusion coefficient (ADC), and it's possible to identify imaging biomarkers for fibrosis, tumor fluid and cell membrane integrity using a mono-exponential model or with diffusion and perfusion parameters in a bi-exponential model [104–114]. Using an Intravoxel Incoherent Motion method (IVIM) bi-exponential model to analyze DWI data, it is possible to obtain the pure tissue coefficient (Dt) linked only to diffusion water mobility, the pseudo-diffusion coefficient (Dp) linked to blood mobility, and the perfusion fraction (fp) [115–122]. The traditional DWI data analysis approach is founded on the hypothesis that voxel water diffusion has a single component and follows a normal Gaussian distribution, and that water molecules diffuse without any constraint. However, water molecule diffusion within biologic tissue exhibits non-Gaussian behavior [123–132]. Jensen et al. in 2005 reported a non-Gaussian diffusion model called Diffusion Kurtosis imaging (DKI) [123] used to analyze DWI data. This model includes the mean value of the kurtosis median coefficient (MK), which measures the tissue diffusion deviation from a Gaussian model, and the mean value of the diffusion coefficient (MD) with the correction of the non-Gaussian bias [123].

The role of DWI and functional parameters obtained by DWI in HCC has been assessed by different studies. Lee et al. [133] showed that DWI allowed to differentiate between HCCs and dysplastic nodules. They found that 86 HCCs (84.3%) showed hyperintensity on DWI, conversely, only 3 dysplastic nodules had this feature. Piana et al. [134] showed that restricted signal on DWI sequences and hyperenhancement during arterial phase

were more sensitive than conventional vascular criteria. DWI could be used as a helpful tool for HCC in patients with chronic liver disease, since it can accurately detect HCC in patients with chronic liver disease regardless of the lesion size [134–136]. However, several researchers [137] have shown that DWI not allow to differentiate HCC from other hepatic lesions, since these solid lesions also have increased cellularity, showing ADC values that overlap with ADC values of HCC.

Recently, non-Gaussian diffusion behavior has been described in HCC and several authors have also evaluated the utility of the non mono-exponential models for the characterization and the assessment of treatment response in HCC patients [138–140]. However, the knowledge is still limited on which non mono-exponential model could more accurately evaluate the non-Gaussian DWI signal.

The pathological grade of HCC is connected to the prognosis, and it is one of the independent predictive features for recurrence and long-term survival after hepatic resection [141, 142]. However, it is challenging to define accurate preoperative grade using imaging modalities. Several studies [13, 117, 143–145] have assessed the role of several parameters by DWI and histological grade of HCC. Chen et al. [145], in a meta-analysis, found that for distinguishing well differentiated nodules from higher grades, DWI showed a low sensitivity (54%), high specificity (90%), and an excellent diagnostic performance. Conversely, in differentiating poorly differentiated nodules from lower grades, the sensitivity was 84%, the specificity 48%, showing a moderately high diagnostic performance. Granata et al. [117] found that DWI could be used to predict the histological grade of HCC; in fact, they showed that there was a good correlation between ADC and grading, between perfusion fraction (*fp*) and grading, and between tissue pure diffusivity (*Dt*) and grading.

Bold-MRI

Hypoxia is emerging as a key factor of the aggressive tumor biology and the relative resistance to conventional as well as targeted therapies [146]. Several factors contribute to the low oxygen tension. Among these are its characteristically low microvascular density, rapid tumor growth which may result in impaired architecture of the tumor vessels, as well as the extensive desmoplastic stroma that exerts mechanical stress on the tumor vasculature and thus impairing tissue perfusion [146].

The only noninvasive imaging method that can reflect in vivo blood oxygen level is blood oxygen level-dependent (BOLD) functional magnetic resonance imaging (fMRI). BOLD MRI makes use of paramagnetic properties of deoxyhemoglobin and is mainly used for regional quantification of oxygenation [146]. The specific imaging mechanism is as follows: iron ions of deoxyhemoglobin contain unpaired electrons and have a paramagnetic property that shortens the transverse relaxation time of nearby protons. This is reflected in tissue T2-star (T2*) value, which is negatively correlated with the deoxyhemoglobin concentration [146]. With the evolution of hepatic fibrosis, progressive disruption of normal liver architecture is seen, which gives rise to regional and global changes in perfusion. Venous flow typically decreases due to increased resistance in the portal venous system, and may bypass the parenchyma completely via portosystemic venous shunts. Hepatic arterial flow commonly increases to counteract this effect. Impaired hemodynamic response and increased arterial blood flow to the liver may account for the elevated T2* response seen in diseased liver tissue. This is consistent with a breakdown in autoregulatory function, and is similar to the reduced hemodynamic response to carbogen challenge [147, 148]. Measuring native T2* or change in T2*, in response to a hyperoxic stimulus has been proposed as an intrinsic marker of tumor oxygenation, and T2* is proportional to the concentration of deoxyhemoglobin, which in turn relates to arterial blood pO2.

BOLD assessment is an useful tool in the hepatocarcinogenesis process so as after local treatment.

Petterson et al. [147] observed a larger but more variable response to oxygen challenge in HCC, which may be expected given variations in oxygenation and perfusion, even within the same tumor type. The initial pathogenesis of HCC involves an increased arterial supply; however, in late-stage HCC the arterial blood supply may decrease. This variability in blood supply, and the consequent proportions of oxyhemoglobin, could be a source of variability in the observed BOLD response [147].

Tumoral changes caused by TACE such as tumor vascularity, blood supply ratio of the hepatic artery to the portal vein, and aerobic metabolic activity may be assessed by BOLD-fMRI [149]. This technique may thus serve as a novel and useful noninvasive functional biomarker for assessing the early T2* changes post-TACE. TACE reduced the BOLD response in the cancerous area by blocking the blood supply to the tumor [149]. In preliminary rabbit VX2 liver tumor oxygenation experiments, Rhee et al. demonstrated a statistically significant decrease in the T2* value after TACE with polyvinyl alcohol particles [150]. Choi et al. reported that TACE induced a significant reduction in the Δ R2* values of tumors on the first day after the procedure [151].

Radiomics analysis

Radiomics consists of the extraction of several parameters by radiological data that can provide information about tumor phenotype as well as the cancer microenvironment [152–160]. Radiomics, when combined

with other data linked to patient outcome, can produce precise evidence-basedclinical-decision support systems. The main task is to combine and to collect differents multimodal quantitative data with a mathematical method in order to provide clear and robust clinical parameters and to allow outcome prediction [68]. The idea of radiomics is that the quantitative variables are more sensitively correlated with various clinical endpoints compared with qualitative radiologic and clinical data. Radiomics offer outstanding benefits over qualitative imaging assessment, since this is clearly limited by the resolution of radiologist 'eyes [161–164]. A radiomic information extension can be obtained by adding genomics data (radiogenomics); in fact, genomic markers such as microRNA expression, have been shown associated with treatment response, metastatic spread and prognosis that could offer personalized and precision medicine [68]. Radiogenomics could perform patient selection for different cancer therapy, predict therapy, address potential therapy resistance (chemotherapy and/or radiation-therapy) and select patients with poor prognosis [68].

The framework of radiomic analysis mainly involves four phases: acquisition of the image, identification of a region of interest (manually or automatically), segmentation, and feature selection, model building, and classification. The approaches applied to evaluate radiomic traits are classified into three types including statistics-based, model-based, and transform-based [68].

To date, several studies have evaluated the radiomic or radiogenomic traits and factors affecting the survival of patients with HCC after chemotherapy, resection, interventional treatments, and transplantation through non-invasive imaging, and have highlighted the significance of non-invasive method in evaluating these prognostic factors [165]. The radiomic studies, assessing the relationship between imaging traits and clinical characteristics including survival, recurrence, or treatment response of HCC, have been greatly studied by CT. By contrast, relatively few studies have dealt with these relationships by MRI images. This may be due to the difficulty of providing standardization of MR images compared with CT imaging. In fact, MRI provides the advantage of high-contrast structural and functional information illustrating soft-tissue characteristics, and the technique is superior in assessing the tumor's metabolism and proliferation with higher accuracy. Metabolic imaging using 18-fluoro-deoxyglucose positron emission tomography (FDG-PET) has also been used to demonstrate the prognostic value of radiomics in HCC [166].

The areas of greatest interest were related to the characterization of the lesions [167–173] and the evaluation of the response to therapy [174–182].

For the differentiation between HCC and benign hepatic lesions, a CT-based radiomics nomogram, which incorporated the rad-score and clinical factors showed an area under the receiver operating characteristic curve (AUC) of 0.917 for differentiating FNH from HCC [183]. An MRI-based study in 369 patients with 446 lesions (HCC 222, hemangioma 224) reported an AUC of 0.89 (sensitivity 0.822, specificity 0.714) for differentiating between HCC and hemangioma using images with in-phase, out-phase, T2-weighted, and diffusion-weighted imaging sequences [184]. In addition, according to a more recent study with both CT and MRI, fusion models that simultaneously integrated clinical characteristics achieved average AUCs of 0.966 (CT) and 0.971 (MRI), with 10-foldcross-validation to differentiate hepatic epithelioid angiomyolipoma from HCC and FNH [185]. Furthermore, a multicenter retrospective cohort study performed in 178 cirrhosis patients (with indeterminate liver nodules including other malignant lesions as cholangiocarcinoma and metastasis, regenerative nodule, hemangioma and FNH) reported an AUC of 0.66 to diagnose HCC using triphasic contrast-enhanced CT, and suggested the benefit of AI to enhance clinicians' decisions by identifying a subgroup of patients with high HCC risk [169].

Several studies suggest the effect of radiomics-based data to help make treatment decisions by the noninvasive prediction of the response to TACE and immune-oncologic features [174–182]. Thus, if the therapeutic direction is considered to be unresponsive to TACE, it may be changed to the use of molecular targeted agents (i.e., sorafenib). However, the practical benefit of radiomics-based findings needs to be validated by additional studies in a prospective setting.

Although radiomics is not a panacea for clinical management, it is an up-and-coming and highly relevant method in cancers and in diseases other than malignancy such as neurological and vascular pathologies [156, 186, 187].

Diagnostic management-Li-RADS

HCC may be noninvasively diagnosed by imaging findings alone, often without biopsy [188]. To standardized imaging and reporting, the American College of Radiology (ACR) developed LI-RADS at CT or MRI in patients at risks for HCC in 2011, which has been refined and expanded over multiple updates to version 2018 till now to consist with clinical practice, such as introducing the concept of LR-OM for non-HCC malignancies in 2013, which was renamed as LR-M in 2014 [189–191]. Besides, CEUS highlights itself with a real-time observation, for which ACR established the CEUS LI-RADS in 2016 and further revised LR-M observations in 2017 [192–194]. Several studies showed the value of LR-M observation for differentiating non-HCC malignancies from HCC. An et al. [195] found that CT and MRI

showed comparable capabilities for distinguishing non-HCC malignancies from HCC based on CT/MRI LI-RADS, with pooled accuracies of 79.9 and 82.4% for categorizing LR-M. Kim et al. [196] demonstrated that non-HCC malignancy could be distinguished from HCC at a sensitivity of 89% and a specificity of 48% in patients with liver cirrhosis by using the LR-M criteria of CT/MRI LI-RADS v2018 at gadoxetate-enhanced MRI. Zheng et al. [197] validated the CEUS LI-RADS by showing a sensitivity of 89% and a specificity of 88% for the LR-M category to distinguish non-HCC malignancy from HCC. Due to good diagnostic performance, CT/MRI LI-RADS was integrated into HCC guidance from American Association for the Study of Liver Diseases (AASLD) in 2018 [198]. However, AASLD does not accept CEUS as a diagnostic technique but a second-line technique after CT or MRI [198].

LI-RADS offers four individual imaging algorithms designed for different clinical contexts: *(a)* US LI-RADS for surveil- lance, *(b)* CT/MRI LI-RADS for diagnosis and staging, *(c)* CEUS LI-RADS for diagnosis, and *(d)* treatment response LI-RADS to assess response to local-regional therapies [198].

LI-RADS defines eight unique diagnostic categories based on imaging appearance that reflect the probability of HCC or malignancy with or without tumor in vein. The category LR-NC (not categorizable) is applied when image omission or degradation precludes categorization. The categories LR-1 (definitely benign) and LR-2 (probably benign) range from simple cysts to LR-2 distinctive nodules. An LR-2 distinctive nodule is defined by its size (< 20 mm) and the absence of any major features of HCC, any features of LR-M, or any ancillary features of malignancy [198]. LR-3 (intermediate probability of HCC) includes some perfusion alterations that have a nodular shape and true nodules with one or two malignant features. The malignant categories range from probable to definite malignancy and include LR-4 (probably HCC), LR-5 (definitely HCC), LR-M (probably or definitely malignant, not specific for HCC), and LR- TIV (malignancy with tumor in vein) [198].

The LI-RADS lexicon divides imaging features into major features, LR-M features, and ancillary features. Major features include nonrim APHE, nonperipheral "washout" appearance, enhancing "capsule" appearance, size, and threshold growth [198]. LR-M features include a targetoid or nontargetoid mass with one or more of the following findings: infiltrative appearance, marked diffusion restriction, necrosis, or other features suggestive of non-HCC malignancy [198]. Ancillary features are divided into those favoring benignity, those favoring malignancy, and those favoring HCC. Their use is optional, and they may be used to up or downgrade a category by one, but they cannot be used to upgrade to LR-5 [198].

Multiphase contrast-enhanced imaging is necessary to assess LI-RADS features. Intravenous extracellular contrast agents are used for CT, while those used for MRI may be extracellular or hepatobiliary. Both gadoxetate disodium and gadobenate dimeglumine may be used in hepatobiliary phase imaging. For treatment-naive patients undergoing CT, unenhanced imaging is optional; however, it is required in the post treatment setting for CT and all MRI studies. Late arterial phase is strongly preferred over early arterial phase [198].

The choice of modality (CT or MRI) and MRI contrast agent (extracelllar or hepatobiliary) depends on patient, institutional, and regional factors. LI-RADS does not endorse any particular imaging method, rather, it provides guidance on technique, terminology, interpretation, and reporting [198].

CEUS is most suitable for problem solving, categorizing individual observations, and differentiating tumor in vein from bland thrombus rather than for staging the entire liver. CEUS requires expertise and specialized equipment [198].

Ablation techniques assessment

The primary endpoint of ablation therapy is to obtain a complete necrosis (similar to R0 resection) of liver tumors that is linked to create a safety margin of at least 10 mm round the external margin of the lesion. However, the effectiveness of the treatment is linked to numerous features, such as tumor size, location, blood flow, and equipment utilized [14]. RFA and MWA are hyperthermic techniques [14, 199]. RFA produces necrosis thanks to thermocoagulation. With RFA, the zone of active tissue heating is restricted to a few millimetres nearby to the electrode, with the residue of the target being heated via thermal conduction [14, 199]. Consequently, the treatment efficacy is closely related to the lesion size, and the maximum result is obtained for target less than 3.5 cm [14, 199]. Additionally, some tissue features, such as electrical conductivity, thermal conductivity, dielectric permittivity, and blood perfusion rate, have effect on the efficacy of RFA procedure.

MWA uses the dielectric effect, which occurs when an imperfect dielectric material is subjected to an alternating electromagnetic (EM) field, generating a larger area of active heating (up to 2 cm close the antenna) allowing more homogeneous necrosis in the target zone, compared to RFA [199]. Conversely, to RFA and MWA, IRE and ECT are non-thermal techniques that cause ablation changing cell membrane permeability thanks to an induced electric field (electroporation).

IRE is considered as a direct ablation tool, since electroporation is used in irreversible manner [199]. Short high-voltage electric current fields cause the irreversible permeabilization of the lipid bilayer, the disruption of

the cellular homeostasis, and the stimulation of apoptotic pathways, causing death of neoplastic cells [199]. Taking into account its mechanism of action, IRE can protect surrounding structures, such the vessels and bilir tree [199].

Among all the ablative procedures, RFA is a frontline technique for HCCs smaller than 20 mm [14]. Several studies have evaluated the efficacy of RFA with respect to resection and have established that RFA is a noninvasive and effective ablative treatment [200–204]. Although these studies focused on RFA as a stand-alone therapy contained valuable information regarding treatment safety and response, they lacked sufficient follow-up to define important long-term outcomes such as survival. Only recently have survival data become available on RFA-treated patients with HCC. Large clinical series from Europe, the U.S., and Asia have demonstrated 5-yearpost-RFA survival rates between 33 and 55%, comparable to those seen in series of hepatic resection [205].

With the microwave technology progress and a continuously cooled electrode development, MWA has recently been used more recurrently in treatment of HCC [206–208]. According to the pubblished data, overall survival, local recurrence, complication rates, disease-free survival, and mortality in patients with HCC treated with MWA (compared with RFA) vary between 22 months for focal lesion > 3 cm (vs. 21 months) and 50 months for focal lesion ≤3 cm (vs. 27 months), between 5% (vs. 46.6%) and 17.8% (vs. 18.2%), between 2.2% (vs. 0%) and 61.5% (vs. 45.4%), between 14 months (vs. 10.5 months) and 22 months (vs. no data reported), and between 0% (vs. 0%) and 15% (vs. 36%), respectively [14].

Postablation imaging is necessary to assess the treatment results, to monitor evolution of the ablated tissue over time, and to evaluate for complications [209]. Post-thermal treatments, imaging should be performed at regularly scheduled intervals to assess treatment response and to evaluate for new lesions and potential complications. Although there is no widely accepted post-treatments imaging surveillance protocol, the protocol should include 1-, 3-, 6-, 9-, and 12-monthcontrast-enhanced CT or MRI follow up. Periablation enhancement that occurs as a result of inflammation in the surrounding parenchyma and that could depict residual disease gradually decreases over time [210].

On unenhanced CT performed closly after thermal treatment, the ablation zone is larger than the initial target and is hypoattenuating or heterogeneously hyperattenuating because of coagulative necrosis and hemorrhagic products; however, occasionally no visible changes may be discernible on CT [210]. At the first follow-up CECT or MRI evaluation, the ablation zone can be spherical, oval, or oblong dependent on the number and type of electrodes used. For lesion located between blood vessels, the shape of the ablation zone post RFA can be irregular because of the "heat sink" effect. On unenhanced CT, the ablation zone becomes more homogeneously hypoattenuating over time. On MRI, the treated leion is heterogeneously or peripherally hyperintense on T1-weighted images and heterogeneous or hypointense on T2-weighted because of coagulative necrosis, hemorrhagic products, and dehydration. These changes can persist for variable periods of time; the imaging appearances change as the blood products evolve and also become more homogeneous over time. Marked hyperintensity on T2-weighted imaging suggests liquefactive necrosis or biloma formation. On CECT and MRI, the ablation zone is well demarcated and no enhancement suggests a lack of viable tumor [210]. CEUS has been employed in the early assessment of the ablated HCC, being comparable to CT and MRI in the detection of residual viable tumor [211]. However, the potential role of CEUS in the follow-up of the patient with a successful ablation has not been adequately investigated. CEUS is indicated in the assessment of local tumor progression when follow-up CT or MR are contraindicated or not conclusive and that, in addition to CT and/or MR, CEUS may be used in follow-up protocols. CEUS has the limitation of being unable to explore the entire liver during the arterial phase, which is a rather limited time frame. Consequently, while CT and MRI allows to scan the whole liver during the arterial phase and to rescan it during the portal and late phase achieving a multiphase study, CEUS may miss a transiently hyperperfused lesion just because not exploring that given liver area in the appropriate moment [211].

IRE is a relatively new minimally invasive image-guided technique for the interventional oncologic treatment of soft tissue tumors. IRE offers several potential advantages over thermal ablation approaches, specifically, a relatively short ablation procedure and the ability to ablate tumors adjacent to large blood vessels. Thus, IRE may be well suited for the ablation of solid organ tumors such as primary or metastatic lesions in the liver, especially those located near blood vessels, bile ducts, and nerves [212]. However, one possible disadvantage of IRE may be its lower success rate for complete local tumor eradication. This may be attributable to the fact that the optimal timing of image-basedfollow-up and the most suitable imaging modality for follow-up have yet to be determined because IRE therapy has only recently been introduced. With regard to this point, another problem is that the contrast-enhanced imaging characteristics of liver tumors that have been successfully treated by IRE ablation differ from those observed following RFA. Specifically, unlike RFA, persistent enhancement of the peritumoral liver parenchyma is

observed within the IRE ablation zone, and thus the ablated margin is not clear in IRE. These are crucial factors for identifying residual tumor and for planning retreatment [212]. Sugimoto et al. evaluated the diagnostic performance of CEUS, CECT and EOB-MRI in the assessment of immediate response to IRE in liver lesions. They found, during the arterial phase of CEUS, EOB-MRI, and CECT images five categories of post IRE lesions, according to their enhancement patterns. The areas under the ROC curve for CEUS were significantly higher than those for EOB-MRI and CECT. The sensitivities and specificities were higher with CEUS than with EOB-MRI and CECT. However, the differences were not statistically significant. Ths study showed that CEUS was the ideal modality for evaluating the treatment response to IRE in the subacute phase (i.e., within 1 week after IRE). Continuous real-time observation of hemodynamic changes in ablated lesions is possible with CEUS because microbubbles are pure intravascular tracers that remain in the blood pool. CEUS is, therefore, very sensitive to the presence of a residual functional vascular bed in the ablated area and can provide information concerning the vessels remaining in the treated area. Moreover, CEUS can be performed immediately after the IRE procedure without difficulty [212].

The contrast enhancement imaging characteristics of successfully IRE-ablated liver tumors are different from those seen in RFA. A previous study in a patient with HCC treated by IRE reported that despite persistent enhancement of peritumoral liver parenchyma within the IRE ablation zone, the tumor itself was clearly demarcated by a devascularized area in comparison to surrounding unablated or ablated liver parenchyma [213]. In our previous study we dscribed the MRI findings of HCC treated with IRE at 1-monthfollow-up [214]. Ablation zones showed a round shape in 20 of 24 treated lesions. Those zones located underneath the hepatic capsule had an oval configuration (4/24; 17%). The ablation zones increased in size by 10% compared with their initial size on pretreatment imaging. On T1-weighted images, all lesions (100%) showed a nonhomogeneous signal, with a hyperintense central core and a hypointense peripheral rim. On T2-weighted sequences, the signal from the necrotic ablation zone was heterogeneously hypointense (Fig. 9). The residual tumor tissue appeared as a peripheral portion that was hypointense on the T1-weighted images and hyperintense on the T2-weighted images. On DWI, twenty out of 24 treated lesions (83%) showed restricted diffusion. On the other hand, when the lesions were not clearly visible at a b value of $0 \, s/mm^2$ (4/24; 17%), there was no signal detectable at a b value of $800 \, mm/s^2$, where only the rim showed restricted diffusion (targetoid appearance) (Fig. 10). The ADC values did not show any statistically significant difference for each single lesion evaluated between baseline and at 1 month, with a large overlap between the ADC values recorded before and after IRE. During the dynamic sequences and the liver-specific phases, the treated area showed hypointensity signal. The ablation zones containing residual viable tumor (2/24; 8.3%) showed contrast enhancement during the arterial phase and portal phase washout. The residual tumor tissue appeared as hypointense, although to a lesser degree than the necrotic portion, in the hepatobiliary phase. In four peripheral treated lesions (17%), there was capsular retraction. Six out of 20 patients (30%) showed a THID area within the normal liver parenchyma adjacent to the treated lesions. Two out of the 20 patients (10%) had no concentration of liver-specific contrast medium around the ablation zone [214].

Few studies describe the radiological findings of ECT on treated liver lesions. The response of a tumour after ECT is slow due to its mode of action, i.e., due to slow killing of the dividing cells that occurs due to the internalization of the bleomycin by electroporation. The treated tumor gradually changes into fibrotic tissue during a period of 4 months [215]. Boc et al., assessed US changes in the liver treated ECT tumors [216]. During the 1st phase took up to 5 min after the delivery of electric pulses. The hyperechoic microbubbles were observed along the electrode tracks and were visible immediately i.e. within a few seconds after the pulses were triggered and later within the entire ablation zone. During the 2nd phase, after 5–15 min, microbubbles were distributed throughout the treated tumor, and the tumor became hyperechoic and surrounded by a hypoechoic zone. The hypoechoic zone (5–15 mm wide) represents the electroporated area within the normal liver tissue represents the treatment safety margin. Four days after ECT, US of the metastasis in patient #1 she presented with an 18-mm hyperechoic formation surrounded by a 5-mm hypoechoic area, which is most likely the oedematous area of the liver parenchyma, or the safety margin. Five months after ECT, US and MRI showed the metastasis in *patient 1* as a fibrotic residuum without the hypoechoic rim. The size of the metastasis was not significantly reduced. The appearance was as a complete response, which was also present 7 months after ECT; however, at that time, the size was significantly reduced to 11 mm from the original 20 mm in the greatest diameter, indicating the slow resorption of the treated metastasis. Similar MRI findings were shown in *patient 2*, 3 months after ECT in which the treated metastasis was reduced from 19 to 13 mm in diameter [216].

Tarantino et al. treated with ECT a prospective case series of patients with liver cirrhosis and Vp3-Vp4- portal vein tumor thrombus (PVTT) from HCC, in order to evaluate the feasibility, safety and efficacy of this
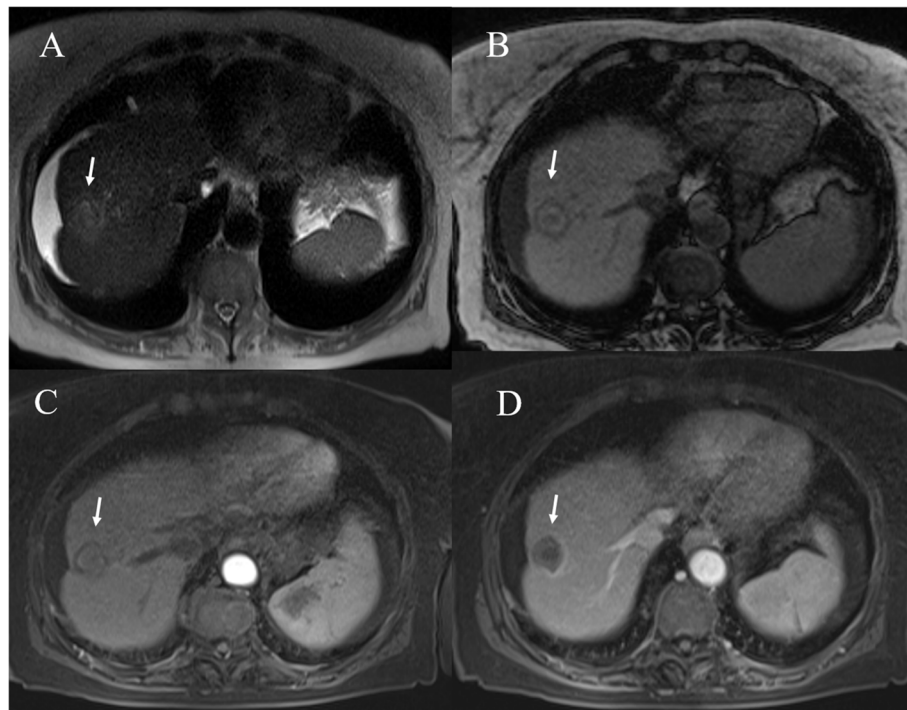
Fig. 9 Post RFA MRI assessment of HCC on VIII hepatic segment. The ablated lesion is non viable with isointense signal in T2-W (**A**) sequence, targetoid appearance in T1-W (**B** and **C**) sequences and no hypeeenhancement during artierial phase (**D**) of contrast study

treatment. Post treatment intraoperative CEUS demonstrated complete absence of enhancement of the thrombosis and of the treated HCC nodule in all cases. The follow-up ranged from 9 to 20 mo (median, 14 mo). In these two patients, CEUS and CT confirmed complete patency of the vessel without any intravascular or perivascular recurrence during follow-up. In three patients, CT and CEUS showed permanent complete thrombosis with a persistent, shrinked, avascular thrombus into the treated vessels. In all three cases, no intravascular or perivascular enhancement consistent with residual tumor or local recurrence was detected at CT and CEUS during follow- up. In the remaining patient, 24 h post-

treatment CEUS showed absence of enhancement of the treated thrombus. However, the patient was lost to follow-up because of death from gastrointestinal hemorrage 5 weeks after ECT treatment [217].

It is clear that, considering therapeutic responses to treatments, imaging data are sometimes complicated to understand because it depend on anatomic location, on the method of act of given therapy, on the morphological and functional criteria that are used for each imaging modality. In this setting, imaging observations depend highly on the type and the method of therapy delivery, the timing of treatment, and the imaging technique being used to observe the effects. Therefore, an
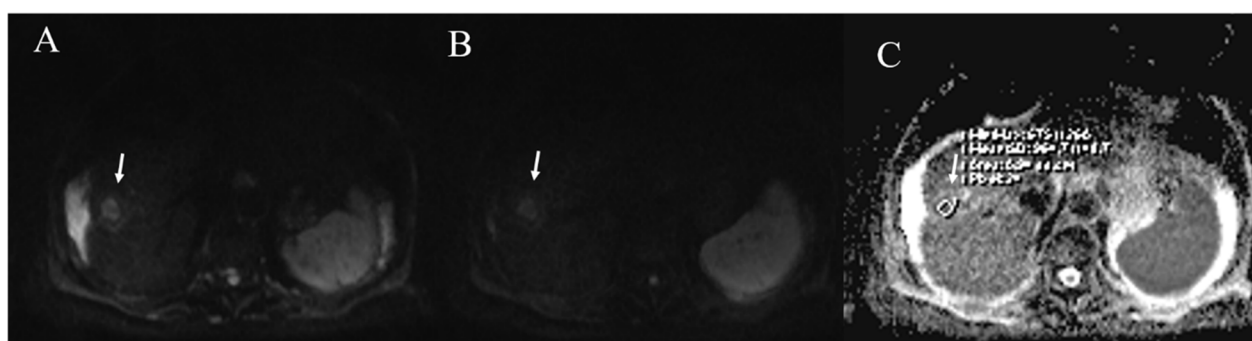

Fig. 10 The same patient of Fig. 9. DWI assessment. The ablated area shows targetoid appearance in b50 s/mm2, in b 800 s/mm^2 and ADC map

Granata *et al. Infectious Agents and Cancer*   (2021) 16:53

Page 15 of 22

evaluation based only on dimensional data is not appropriate to assess the efficacy of such complex treatments, since not always a positive response to treatment is linked to a size reduction; furthermore dimensional criteria do not allow the differentiation of the fibrotic tissue from the residual tumor [218]. The LI-RADS treatment response algorithm applies to multiphase CT or MRI used to assess response after local-regional therapy, which includes percutaneous therapy (eg, ethanol and radiofrequency or microwave ablation), transcatheter therapy (eg, transarterial chemoembolization or radioemboliza- tion), and external beam radiation therapy. The algorithm also applies to observations at the surgical margin after resection of lesion. The LI-RADS treatment response algorithm does not apply to systemic chemotherapies, targeted, and/or immunologic therapies [198].

LI- RADS treatment response category codes reflect the relative probability of tumor viability after local-regional therapy to guide management decisions. Similar to the modified Response Evaluation Criteria in Solid Tumors (mRECIST) [219], the LI-RADS algorithm is based on unidimensional measurements of the largest enhancing component of a treated tumor, excluding areas of nonenhancement.

Conclusion

HCC may be noninvasively diagnosed by morphological and functional imaging. To day, the vascular assessment of focal hepatic nodule allow to identy HCC nodules, so that multiphase contrast-enhanced imaging is necessary during diagnostic phase. Intravenous extracellular contrast agents are used for CT, while those used for MRI may be extracellular or hepatobiliary. Both gadoxetate disodium and gadobenate dimeglumine may be used in hepatobiliary phase imaging. For treatment-naive patients undergoing CT, unenhanced imaging is optional; however, it is required in the post treatment setting for all CT and MRI studies. Regarding to contrast study protocol, late arterial phase is strongly preferred over early arterial phase.

Although the choice of modality (CT, US/CEUS or MRI) and MRI contrast agent (extracelllar or hepatobiliary) depends on patient, institutional, and regional factors. However, MRI allows to link morfological and functional data in the HCC evaluation.

Postablation imaging is necessary to assess the treatment results, to monitor evolution of the ablated tissue over time, and to evaluate for complications. Postthermal treatments, imaging should be performed at regularly scheduled intervals to assess treatment response and to evaluate for new lesions and potential complications. At the first follow-up CECT or MRI evaluation, the ablation zone can be spherical, oval, or oblong dependent on the number and type of electrodes used.

Declarations

Ethics approval and consent to participate
Not applicable.

Consent for publication
Not applicable.

Competing interests
The authors have no conflict of interest to be disclosed.

Author details
[1]Division of Radiology, Istituto Nazionale Tumori IRCCS Fondazione Pascale – IRCCS di Napoli, Naples, Italy. [2]Division of Radiology, Università degli Studi della Campania Luigi Vanvitelli, Naples, Italy. [3]Italian Society of Medical and Interventional Radiology SIRM, SIRM Foundation, Milan, Italy. [4]Medical Oncology Division, Igea SpA, Naples, Italy. [5]Division of Hepatobiliary Surgical Oncology, Istituto Nazionale Tumori IRCCS Fondazione Pascale – IRCCS di Napoli, Naples, Italy. [6]Department of Medicine, Surgery and Dentistry, University of Salerno, Salerno, Italy. [7]Radiology Division, Azienda Ospedaliero-Universitaria Careggi, Florence, Italy. [8]Department of Radiology, UOC San Severo Hospital, San Severo, Italy. [9]Department of Medicine and Health Sciences "Vincenzo Tiberio", University of Molise, Campobasso, Italy. [10]Abdominal Oncology Division, Istituto Nazionale Tumori IRCCS Fondazione Pascale – IRCCS di Napoli, Naples, Italy.

References
1. Sung H, Ferlay J, Siegel RL, Laversanne M, Soerjomataram I, Jemal A, et al. Global cancer statistics 2020: GLOBOCAN estimates of incidence and mortality worldwide for 36 cancers in 185 countries. CA Cancer J Clin. 2021. https://doi.org/10.3322/caac.21660.
2. World Health Organization (WHO). Global Health Estimates 2020: Deaths by cause, age, sex, by country and by region, 2000-2019: WHO; 2020. Accessed 11 Dec 2020
3. Barabino M, Gurgitano M, Fochesato C, Angileri SA, Franceschelli G, Santambrogio R, et al. LI-RADS to categorize liver nodules in patients at risk of HCC: tool or a gadget in daily practice? Radiol Med. 2021;126(1):5–13. https://doi.org/10.1007/s11547-020-01225-8 Epub 2020 May 26. PMID: 32458272.
4. Gabelloni M, Di Nasso M, Morganti R, Faggioni L, Masi G, Falcone A, et al. Application of the ESR iGuide clinical decision support system to the imaging pathway of patients with hepatocellular carcinoma and cholangiocarcinoma: preliminary findings. Radiol Med. 2020;125(6):531–7. https://doi.org/10.1007/s11547-020-01142-w Epub 2020 Feb 4. PMID: 32020528.
5. Granata V, Fusco R, Amato DM, Albino V, Patrone R, Izzo F, et al. Beyond the vascular profile: conventional DWI, IVIM and kurtosis in the assessment of hepatocellular carcinoma. Eur Rev Med Pharmacol Sci. 2020;24(13):7284–93. https://doi.org/10.26355/eurrev_202007_21883 PMID: 32706066.
6. Granata V, Fusco R, Maio F, Avallone A, Nasti G, Palaia R, et al. Qualitative assessment of EOB-GD-DTPA and Gd-BT-DO3A MR contrast studies in HCC

patients and colorectal liver metastases. Infect Agent Cancer. 2019;14:40. https://doi.org/10.1186/s13027-019-0264-3 PMID: 31798677; PMCID: PMC6882051.

7. Gatti M, Calandri M, Bergamasco L, Darvizeh F, Grazioli L, Inchingolo R, et al. Characterization of the arterial enhancement pattern of focal liver lesions by multiple arterial phase magnetic resonance imaging: comparison between hepatocellular carcinoma and focal nodular hyperplasia. Radiol Med. 2020; 125(4):348–55. https://doi.org/10.1007/s11547-019-01127-4 Epub 2020 Jan 8. PMID: 31916102.

8. Orlacchio A, Chegai F, Roma S, Merolla S, Bosa A, Francioso S. Degradable starch microspheres transarterial chemoembolization (DSMs-TACE) in patients with unresectable hepatocellular carcinoma (HCC): long-term results from a single-center 137-patient cohort prospective study. Radiol Med. 2020;125(1):98–106. https://doi.org/10.1007/s11547-019-01093-x Epub 2019 Oct 3. PMID: 31583558.

9. Granata V, Fusco R, Avallone A, Catalano O, Filice F, Leongito M, et al. Major and ancillary magnetic resonance features of LI-RADS to assess HCC: an overview and update. Infect Agent Cancer. 2017;12:23. https://doi.org/10.1186/s13027-017-0132-y PMID: 28465718; PMCID: PMC5410075.

10. Kitao A, Matsui O, Yoneda N, Kozaka K, Kobayashi S, Koda W, et al. Gadoxetic acid-enhanced MR imaging for hepatocellular carcinoma: molecular and genetic background. Eur Radiol. 2020;30(6):3438–47. https://doi.org/10.1007/s00330-020-06687-y Epub 2020 Feb 16. PMID: 32064560.

11. Granata V, Fusco R, Avallone A, Filice F, Tatangelo F, Piccirillo M, et al. Critical analysis of the major and ancillary imaging features of LI-RADS on 127 proven HCCs evaluated with functional and morphological MRI: Lights and shadows. Oncotarget. 2017;8(31):51224–37. https://doi.org/10.18632/oncotarget.17227 PMID: 28881643; PMCID: PMC5584244.

12. Granata V, Fusco R, Filice S, Incollingo P, Belli A, Izzo F, et al. Comment on "State of the art in magnetic resonance imaging of hepatocellular carcinoma": the role of DWI. Radiol Oncol. 2019;53(3):369–70. https://doi.org/10.2478/raon-2019-0031 PMID: 31318697; PMCID: PMC6765167.

13. Granata V, Fusco R, Filice S, Catalano O, Piccirillo M, Palaia R, et al. The current role and future prospectives of functional parameters by diffusion weighted imaging in the assessment of histologic grade of HCC. Infect Agent Cancer. 2018;13:23. https://doi.org/10.1186/s13027-018-0194-5.

14. Izzo F, Granata V, Grassi R, Fusco R, Palaia R, Delrio P, et al. Radiofrequency ablation and microwave ablation in liver tumors: an update. Oncologist. 2019;24(10):e990–e1005. https://doi.org/10.1634/theoncologist.2018-0337 Epub 2019 Jun 19. PMID: 31217342; PMCID: PMC6795153.

15. Tan W, Deng Q, Lin S, Wang Y, Xu G. Comparison of microwave ablation and radiofrequency ablation for hepatocellular carcinoma: a systematic review and meta-analysis. Int J Hyperth. 2019;36(1):264–72. https://doi.org/10.1080/02656736.2018.1562571 Epub 2019 Jan 24. PMID: 30676100.

16. Han J, Fan YC, Wang K. Radiofrequency ablation versus microwave ablation for early stage hepatocellular carcinoma: A PRISMA-compliant systematic review and meta-analysis. Medicine (Baltimore). 2020;99(43):e22703. https://doi.org/10.1097/MD.0000000000022703 PMID: 33120763; PMCID: PMC7581069.

17. Luo W, Zhang Y, He G, Yu M, Zheng M, Liu L, et al. Effects of radiofrequency ablation versus other ablating techniques on hepatocellular carcinomas: a systematic review and meta-analysis. World J Surg Oncol. 2017;15(1):126. https://doi.org/10.1186/s12957-017-1196-2 PMID: 28693505; PMCID: PMC5504820.

18. De Filippo M, Ziglioli F, Russo U, Pagano P, Brunese L, Bertelli E, et al. Radiofrequency ablation (RFA) of T1a renal cancer with externally cooled multitined expandable electrodes. Radiol Med. 2020;125(8):790–7. https://doi.org/10.1007/s11547-020-01175-1 Epub 2020 Mar 21. PMID: 32206984.

19. Arrigoni F, Bruno F, Gianneramo C, Palumbo P, Zugaro L, Zoccali C, et al. Evolution of the imaging features of osteoid osteoma treated with RFA or MRgFUS during a long-term follow-up: a pictorial review with clinical correlations. Radiol Med. 2020;125(6):578–84. https://doi.org/10.1007/s11547-020-01134-w Epub 2020 Feb 10. PMID: 32040718.

20. Laimer G, Schullian P, Jaschke N, Putzer D, Eberle G, Alzaga A, et al. Minimal ablative margin (MAM) assessment with image fusion: an independent predictor for local tumor progression in hepatocellular carcinoma after stereotactic radiofrequency ablation. Eur Radiol. 2020;30(5):2463–72. https://doi.org/10.1007/s00330-019-06609-7 Epub 2020 Jan 30. PMID: 32002642; PMCID: PMC7160081.

21. Schullian P, Putzer D, Laimer G, Levy E, Bale R. Feasibility, safety, and long-term efficacy of stereotactic radiofrequency ablation for tumors adjacent to the diaphragm in the hepatic dome: a case-control study. Eur Radiol. 2020; 30(2):950–60. https://doi.org/10.1007/s00330-019-06399-y Epub 2019 Sep 5. PMID: 31489472; PMCID: PMC6957558.

22. Mitrea D, Badea R, Mitrea P, Brad S, Nedevschi S. hepatocellular carcinoma automatic diagnosis within CEUS and B-Mode ultrasound images using advanced machine learning methods. Sensors (Basel). 2021;21(6):2202. https://doi.org/10.3390/s21062202 PMID: 33801125; PMCID: PMC8004125.

23. Trombadori CML, D'Angelo A, Ferrara F, Santoro A, Belli P, Manfredi R. Radial Scar: a management dilemma. Radiol Med. 2021. https://doi.org/10.1007/s11547-021-01344-w. Epub ahead of print.

24. Argalia G, Tarantino G, Ventura C, Campioni D, Tagliati C, Guardati P, et al. Shear wave elastography and transient elastography in HCV patients after direct-acting antivirals. Radiol Med. 2021. https://doi.org/10.1007/s11547-020-01326-4. Epub ahead of print.

25. Ierardi AM, Gaibazzi N, Tuttolomondo D, Fusco S, La Mura V, Peyvandi F, et al. Deep vein thrombosis in COVID-19 patients in general wards: prevalence and association with clinical and laboratory variables. Radiol Med. 2021;126(5):722–8. https://doi.org/10.1007/s11547-020-01312-w Epub 2021 Jan 19. PMID: 33469817; PMCID: PMC7815188.

26. Fanelli F, Cannavale A, Chisci E, Citone M, Falcone GM, Michelagnoli S, et al. Direct percutaneous embolization of aneurysm sac: a safe and effective procedure to treat post-EVAR type II endoleaks. Radiol Med. 2021;126(2): 258–63. https://doi.org/10.1007/s11547-020-01247-2 Epub 2020 Jul 13. PMID: 32661779.

27. Trimboli P, Castellana M, Virili C, Havre RF, Bini F, Marinozzi F, et al. Performance of contrast-enhanced ultrasound (CEUS) in assessing thyroid nodules: a systematic review and meta-analysis using histological standard of reference. Radiol Med. 2020;125(4):406–15. https://doi.org/10.1007/s11547-019-01129-2 Epub 2020 Jan 22. PMID: 31970579.

28. Patrone R, Granata V, Belli A, Palaia R, Albino V, Piccirillo M, et al. The safety and efficacy of Glubran 2 as bilostatic agent in liver resection. Infect Agent Cancer. 2021;16(1):19. https://doi.org/10.1186/s13027-021-00358-3 PMID: 33726798; PMCID: PMC7968309.

29. Granata V, Fusco R, Setola SV, Avallone A, Palaia R, Grassi R, et al. Radiological assessment of secondary biliary tree lesions: an update. J Int Med Res. 2020;48(6):300060519850398. https://doi.org/10.1177/0300060519850398 PMID: 32597280; PMCID: PMC7432986.

30. Granata V, Fusco R, Catalano O, Avallone A, Palaia R, Botti G, et al. Diagnostic accuracy of magnetic resonance, computed tomography and contrast enhanced ultrasound in radiological multimodality assessment of peribiliary liver metastases. PLoS One. 2017;12(6):e0179951. https://doi.org/10.1371/journal.pone.0179951 PMID: 28632786; PMCID: PMC5478136.

31. Calandri M, Ruggeri V, Carucci P, Mirabella S, Veltri A, Fonio P, et al. Thermal ablation with fusion imaging guidance of hepatocellular carcinoma without conspicuity on conventional or contrast-enhanced US: surrounding anatomical landmarks matter. Radiol Med. 2019;124(10):1043–8. https://doi.org/10.1007/s11547-019-01057-1 Epub 2019 Jul 3. PMID: 31270723.

32. Hu HT, Wang W, Chen LD, Ruan SM, Chen SL, Li X, et al. Artificial intelligence assists identifying malignant versus benign liver lesions using contrast-enhanced ultrasound. J Gastroenterol Hepatol. 2021. https://doi.org/10.1111/jgh.15522. Epub ahead of print.

33. Tagliati C, Argalia G, Polonara G, Giovagnoni A, Giuseppetti GM. Contrast-enhanced ultrasound in delayed splenic vascular injury and active extravasation diagnosis. Radiol Med. 2019;124(3):170–5. https://doi.org/10.1007/s11547-018-0961-9 Epub 2018 Nov 28. PMID: 30488252.

34. Imamura H, Hata J, Takata T. Contrast-enhanced ultrasonographic findings of non-occlusive mesenteric ischemia: a case series. Abdom Radiol. 2021. https://doi.org/10.1007/s00261-021-03002-1. Epub ahead of print.

35. Faccioli N, Foti G, Casagranda G, Santi E, D'Onofrio M. CEUS versus CT angiography in the follow-up of abdominal aortic endoprostheses: diagnostic accuracy and activity-based cost analysis. Radiol Med. 2018; 123(12):904–9. https://doi.org/10.1007/s11547-018-0926-z Epub 2018 Aug 6. PMID: 30084107.

36. Rübenthaler J, Negrão de Figueiredo G, Mueller-Peltzer K, Clevert DA. Evaluation of renal lesions using contrast-enhanced ultrasound (CEUS); a 10-year retrospective European single-centre analysis. Eur Radiol. 2018;28(11): 4542–9. https://doi.org/10.1007/s00330-018-5504-1 Epub 2018 May 9. PMID: 29744641.

Granata *et al. Infectious Agents and Cancer*   (2021) 16:53

Page 17 of 22

37. Cao SE, Zhang LQ, Kuang SC, Shi WQ, Hu B, Xie SD, et al. Multiphase convolutional dense network for the classification of focal liver lesions on dynamic contrast-enhanced computed tomography. World J Gastroenterol. 2020;26(25):3660–72. https://doi.org/10.3748/wjg.v26.i25.3660 PMID: 32742134; PMCID: PMC7366064.

38. Grazioli L, Ambrosini R, Frittoli B, Grazioli M, Morone M. Primary benign liver lesions. Eur J Radiol. 2017;95:378–98. https://doi.org/10.1016/j.ejrad.2017.08.028 Epub 2017 Sep 1. PMID: 28987695.

39. Ravanelli M, Agazzi GM, Tononcelli E, Roca E, Cabassa P, Baiocchi G, et al. Texture features of colorectal liver metastases on pretreatment contrast-enhanced CT may predict response and prognosis in patients treated with bevacizumab-containing chemotherapy: a pilot study including comparison with standard chemotherapy. Radiol Med. 2019;124(9):877–86. https://doi.org/10.1007/s11547-019-01046-4 Epub 2019 Jun 6. PMID: 31172448.

40. Miele V, Piccolo CL, Trinci M, Galluzzo M, Ianniello S, Brunese L. Diagnostic imaging of blunt abdominal trauma in pediatric patients. Radiol Med. 2016; 121(5):409–30. https://doi.org/10.1007/s11547-016-0637-2 Epub 2016 Apr 13. PMID: 27075018.

41. Cicero G, Mazziotti S, Silipigni S, Blandino A, Cantisani V, Pergolizzi S, et al. Dual-energy CT quantification of fractional extracellular space in cirrhotic patients: comparison between early and delayed equilibrium phases and correlation with oesophageal varices. Radiol Med. 2021. https://doi.org/10.1007/s11547-021-01341-z. Epub ahead of print.

42. Bozkurt M, Eldem G, Bozbulut UB, Bozkurt MF, Kılıçkap S, Peynircioğlu B, et al. Factors affecting the response to Y-90 microsphere therapy in the cholangiocarcinoma patients. Radiol Med. 2021;126(2):323–33. https://doi.org/10.1007/s11547-020-01240-9 Epub 2020 Jun 27. PMID: 32594427.

43. Rampado O, Depaoli A, Marchisio F, Gatti M, Racine D, Ruggeri V, et al. Effects of different levels of CT iterative reconstruction on low-contrast detectability and radiation dose in patients of different sizes: an anthropomorphic phantom study. Radiol Med. 2021;126(1):55–62. https://doi.org/10.1007/s11547-020-01228-5 Epub 2020 Jun 3. PMID: 32495272.

44. Shin N, Choi JA, Choi JM, Cho ES, Kim JH, Chung JJ, et al. Sclerotic changes of cavernous hemangioma in the cirrhotic liver: long-term follow-up using dynamic contrast-enhanced computed tomography. Radiol Med. 2020; 125(12):1225–32. https://doi.org/10.1007/s11547-020-01221-y Epub 2020 May 15. PMID: 32415477.

45. Bottari A, Silipigni S, Carerj ML, Cattafi A, Maimone S, Marino MA, et al. Dual-source dual-energy CT in the evaluation of hepatic fractional extracellular space in cirrhosis. Radiol Med. 2020;125(1):7–14. https://doi.org/10.1007/s11547-019-01089-7 Epub 2019 Oct 5. PMID: 31587181.

46. Lucatelli P, De Rubeis G, Basilico F, Ginanni Corradini L, Corona M, Bezzi M, et al. Sequential dual-phase cone-beam CT is able to intra-procedurally predict the one-month treatment outcome of multi-focal HCC, in course of degradable starch microsphere TACE. Radiol Med. 2019;124(12):1212–9. https://doi.org/10.1007/s11547-019-01076-y Epub 2019 Aug 31. PMID: 31473930.

47. Granata V, Fusco R, de Lutio di Castelguidone E, Avallone A, Palaia R, Delrio P, et al. Diagnostic performance of gadoxetic acid-enhanced liver MRI versus multidetector CT in the assessment of colorectal liver metastases compared to hepatic resection. BMC Gastroenterol. 2019; 19(1):129. https://doi.org/10.1186/s12876-019-1036-7 PMID: 31340755; PMCID: PMC6651923.

48. Schraml C, Kaufmann S, Rempp H, Syha R, Ketelsen D, Notohamiprodjo M, et al. Imaging of HCC-current state of the art. Diagnostics (Basel). 2015;5(4): 513–45. https://doi.org/10.3390/diagnostics5040513 PMID: 26854169; PMCID: PMC4728473.

49. Hennedige T, Venkatesh SK. Imaging of hepatocellular carcinoma: diagnosis, staging and treatment monitoring. Cancer Imaging. 2013;12(3):530–47. https://doi.org/10.1102/1470-7330.2012.0044 PMID: 23400006; PMCID: PMC3666429.

50. Agostini A, Borgheresi A, Mari A, Floridi C, Bruno F, Carotti M, et al. Dual-energy CT: theoretical principles and clinical applications. Radiol Med. 2019; 124(12):1281–95. https://doi.org/10.1007/s11547-019-01107-8 Epub 2019 Dec 2. PMID: 31792703.

51. Werner S, Krauss B, Haberland U, Bongers M, Starke U, Bakchoul T, et al. Dual-energy CT for liver iron quantification in patients with haematological disorders. Eur Radiol. 2019;29(6):2868–77. https://doi.org/10.1007/s00330-018-5785-4 Epub 2018 Nov 7. PMID: 30406312.

52. Okamura T, Yamada Y, Yamada M, Yamazaki A, Shiraga N, Jinzaki M. Image quality of virtual monochromatic images obtained using 320-detector row

53. Schicchi N, Fogante M, Palumbo P, Agliata G, Esposto Pirani P, Di Cesare E, et al. The sub-millisievert era in CTCA: the technical basis of the new radiation dose approach. Radiol Med. 2020;125(11):1024–39. https://doi.org/10.1007/s11547-020-01280-1 Epub 2020 Sep 15. PMID: 32930945.

54. Yoo J, Lee JM, Yoon JH, Joo I, Lee ES, Jeon SK, et al. Comparison of low kVp CT and dual-energy CT for the evaluation of hypervascular hepatocellular carcinoma. Abdom Radiol. 2021. https://doi.org/10.1007/s00261-020-02888-7. Epub ahead of print.

55. Agostini A, Borgheresi A, Carotti M, Ottaviani L, Badaloni M, Floridi C, et al. Third-generation iterative reconstruction on a dual-source, high-pitch, low-dose chest CT protocol with tin filter for spectral shaping at 100 kV: a study on a small series of COVID-19 patients. Radiol Med. 2021;126(3):388–98. https://doi.org/10.1007/s11547-020-01298-5 Epub 2020 Oct 12. PMID: 33044732; PMCID: PMC7548313.

56. Kim TM, Lee JM, Yoon JH, Joo I, Park SJ, Jeon SK, et al. Prediction of microvascular invasion of hepatocellular carcinoma: value of volumetric iodine quantification using preoperative dual-energy computed tomography. Cancer Imaging. 2020;20(1):60. https://doi.org/10.1186/s40644-020-00338-7 PMID: 32811570; PMCID: PMC7433153.

57. Greffier J, Frandon J, Hamard A, Teissier JM, Pasquier H, Beregi JP, et al. Impact of iterative reconstructions on image quality and detectability of focal liver lesions in low-energy monochromatic images. Phys Med. 2020;77: 36–42. https://doi.org/10.1016/j.ejmp.2020.07.024 Epub 2020 Aug 6. PMID: 32771702.

58. Yoon JH, Chang W, Lee ES, Lee SM, Lee JM. Double Low-dose dual-energy liver CT in patients at high-risk of HCC: a prospective, randomized, single-center study. Invest Radiol. 2020;55(6):340–8. https://doi.org/10.1097/RLI.0000000000000643 PMID: 31917765.

59. Megibow AJ. Clinical abdominal dual-energy CT: 15 years later. Abdom Radiol (NY). 2020;45(4):1198–201. https://doi.org/10.1007/s00261-019-02250-6 PMID: 31583445.

60. Park SH, Kim YS, Choi J. Dosimetric analysis of the effects of a temporary tissue expander on the radiotherapy technique. Radiol Med. 2021;126(3): 437–44. https://doi.org/10.1007/s11547-020-01297-6 Epub 2020 Oct 6. PMID: 33025303.

61. Kim BH, Kim JS, Kim KH, Moon HJ, Kim S. Clinical significance of radiation dose-volume parameters and functional status on the patient-reported quality of life changes after thoracic radiotherapy for lung cancer: a prospective study. Radiol Med. 2021;126(3):466–73. https://doi.org/10.1007/s11547-020-01273-0 Epub 2020 Sep 5. PMID: 32889704.

62. European Association for the Study of the Liver. Electronic address: easloffice@easloffice.eu; European Association for the Study of the Liver. EASL Clinical Practice Guidelines: Management of hepatocellular carcinoma. J Hepatol. 2018;69(1):182–236. https://doi.org/10.1016/j.jhep.2018.03.019. Epub 2018 Apr 5. Erratum in: J Hepatol. 2019;70(4):817.

63. Lencioni R, Fattori R, Morana G, Stacul F. Contrast-induced nephropathy in patients undergoing computed tomography (CONNECT) - a clinical problem in daily practice? A multicenter observational study. Acta Radiol. 2010;51(7): 741–50. https://doi.org/10.3109/02841851.2010.495350 PMID: 20707658.

64. Pang G, Shao C, Lv Y, Zhao F. Tumor attenuation and quantitative analysis of perfusion parameters derived from tri-phasic CT scans in hepatocellular carcinoma: Relationship with histological grade. Medicine (Baltimore). 2021; 100(16):e25627. https://doi.org/10.1097/MD.0000000000025627 PMID: 33879737; PMCID: PMC8078312.

65. Perl RM, Portugall J, Hinterleitner C, Hinterleitner M, Kloth C, Walter SS, et al. Differences between CT-perfusion and biphasic contrast-enhanced CT for detection and characterization of hepatocellular carcinoma: potential explanations for discrepant cases. Anticancer Res. 2021;41(3):1451–8. https://doi.org/10.21873/anticanres.14903 PMID: 33788737.

66. Stella SF, Noel-Lamy M, Rogalla P, Beecroft R, Rajan DK. Hepatic arterial blood flow modulation in patients with hepatocellular carcinoma: a pilot study of the influence of Intraarterial norepinephrine assessed with CT perfusion. J Vasc Interv Radiol. 2021;32(2):204–10. https://doi.org/10.1016/j.jvir.2020.08.006 Epub 2020 Dec 23. PMID: 33358329.

67. Mathew RP, Sam M, Raubenheimer M, Patel V, Low G. Hepatic hemangiomas: the various imaging avatars and its mimickers. Radiol Med. 2020;125(9):801–15. https://doi.org/10.1007/s11547-020-01185-z Epub 2020 Apr 5. PMID: 32249391.

Granata *et al. Infectious Agents and Cancer*   (2021) 16:53

Page 18 of 22

68. Granata V, Fusco R, Avallone A, De Stefano A, Ottaiano A, Sbordone C, Brunese L, Izzo F, Petrillo A. Radiomics-Derived data by contrast enhanced magnetic resonance in RAS mutations detection in colorectal liver metastases. Cancers (Basel). 2021;13(3):453. https://doi.org/10.3390/cancers13030453.

69. Esposito A, Buscarino V, Raciti D, Casiraghi E, Manini M, Biondetti P, et al. Characterization of liver nodules in patients with chronic liver disease by MRI: performance of the liver imaging reporting and data system (LI-RADS v.2018) scale and its comparison with the Likert scale. Radiol Med. 2020; 125(1):15–23. https://doi.org/10.1007/s11547-019-01092-y Epub 2019 Oct 5. PMID: 31587182.

70. Orsatti G, Zucchetta P, Varotto A, Crimì F, Weber M, Cecchin D, et al. Volumetric histograms-based analysis of apparent diffusion coefficients and standard uptake values for the assessment of pediatric sarcoma at staging: preliminary results of a PET/MRI study. Radiol Med. 2021. https://doi.org/10.1007/s11547-021-01340-0 Epub ahead of print.

71. Fusco R, Granata V, Petrillo A. Introduction to special issue of radiology and imaging of cancer. Cancers (Basel). 2020;12(9):2665. https://doi.org/10.3390/cancers12092665 PMID: 32961946; PMCID: PMC7565136.

72. Cholangiocarcinoma Working Group. Italian clinical practice guidelines on Cholangiocarcinoma - part I: classification, diagnosis and staging. Dig Liver Dis. 2020;52(11):1282–93. https://doi.org/10.1016/j.dld.2020.06.045 Epub 2020 Sep 4. PMID: 32893173.

73. Granata V, Fusco R, Venanzio Setola S, Mattace Raso M, Avallone A, De Stefano A, et al. Liver radiologic findings of chemotherapy-induced toxicity in liver colorectal metastases patients. Eur Rev Med Pharmacol Sci. 2019; 23(22):9697–706. https://doi.org/10.26355/eurrev_201911_19531 PMID: 31799635.

74. Liu LH, Zhou GF, Lv H, Wang ZC, Rao SX, Zeng MS. Identifying response in colorectal liver metastases treated with bevacizumab: development of RECIST by combining contrast-enhanced and diffusion-weighted MRI. Eur Radiol. 2021. https://doi.org/10.1007/s00330-020-07647-2. Epub ahead of print.

75. Granata V, Fusco R, Setola SV, Castelguidone ELD, Camera L, Tafuto S, et al. The multidisciplinary team for gastroenteropancreatic neuroendocrine tumours: the radiologist's challenge. Radiol Oncol. 2019;53(4):373–87. https://doi.org/10.2478/raon-2019-0040 PMID: 31652122; PMCID: PMC6884929.

76. Cervelli R, Cencini M, Buonincontri G, Campana F, Cacciato Insilla A, Aringhieri G, et al. 7-T MRI of explanted liver and ex-vivo pancreatic specimens: prospective study protocol of radiological-pathological correlation feasibility (the EXLIPSE project). Eur Radiol Exp. 2020;4(1):58. https://doi.org/10.1186/s41747-020-00185-y PMID: 33057851; PMCID: PMC7560686.

77. Zhao J, Gao S, Sun W, Grimm R, Fu C, Han J, et al. Magnetic resonance imaging and diffusion-weighted imaging-based histogram analyses in predicting glypican 3-positive hepatocellular carcinoma. Eur J Radiol. 2021;139: 109732. https://doi.org/10.1016/j.ejrad.2021.109732 Epub ahead of print. PMID: 33905978.

78. Tang M, Zhou Q, Huang M, Sun K, Wu T, Li X, et al. Nomogram development and validation to predict hepatocellular carcinoma tumor behavior by preoperative gadoxetic acid-enhanced MRI. Eur Radiol. 2021. https://doi.org/10.1007/s00330-021-07941-7. Epub ahead of print.

79. Kulali F, Acar A, Semiz-Oysu A, Canbak T, Tolan K, Bukte Y. Misleading findings of liver-specific MR contrast agent for radiological diagnosis of cysto-biliary communication in hydatid cysts. Radiol Med. 2019;124(6):460–6. https://doi.org/10.1007/s11547-019-01000-4 Epub 2019 Feb 6. PMID: 30725396.

80. Kumada T, Toyoda H, Yasuda S, Sone Y, Ogawa S, Takeshima K, et al. Prediction of hepatocellular carcinoma by liver stiffness measurements using magnetic resonance elastography after eradicating hepatitis C virus. Clin Transl Gastroenterol. 2021;12(4):e00337. https://doi.org/10.14309/ctg.0000000000000337 PMID: 33888672; PMCID: PMC8078363.

81. Kong C, Zhao Z, Chen W, Lv X, Shu G, Ye M, et al. Prediction of tumor response via a pretreatment MRI radiomics-based nomogram in HCC treated with TACE. Eur Radiol. 2021. https://doi.org/10.1007/s00330-021-07910-0. Epub ahead of print.

82. Aslam A, Kamath A, Spieler B, Maschiocchi M, Sabottke CF, Chernyak V, et al. Assessing locoregional treatment response to hepatocellular carcinoma: comparison of hepatobiliary contrast agents to extracellular contrast agents. Abdom Radiol. 2021. https://doi.org/10.1007/s00261-021-03076-x. Epub ahead of print.

83. Park YN, Kim MJ. Hepatocarcinogenesis: imaging-pathologic correlation. Abdom Imaging. 2011;36:232–43.

84. Berardo S, Sukhovei L, Andorno S, Carriero A, Stecco A. Quantitative bone marrow magnetic resonance imaging through apparent diffusion coefficient and fat fraction in multiple myeloma patients. Radiol Med. 2021; 126(3):445–52. https://doi.org/10.1007/s11547-020-01258-z Epub 2020 Aug 18. PMID: 32812173.

85. Golfieri R, Garzillo G, Ascanio S, Renzulli M. Focal lesions in the cirrhotic liver: their pivotal role in gadoxetic acid-enhanced MRI and recognition by the Western guidelines. Dig Dis. 2014;32(6):696–704.

86. Crimì F, Capelli G, Spolverato G, Bao QR, Florio A, Milite Rossi S, et al. MRI T2-weighted sequences-based texture analysis (TA) as a predictor of response to neoadjuvant chemo-radiotherapy (nCRT) in patients with locally advanced rectal cancer (LARC). Radiol Med. 2020;125(12):1216–24. https://doi.org/10.1007/s11547-020-01215-w Epub 2020 May 14. PMID: 32410063.

87. Golfieri R, Grazioli L, Orlando E, et al. Which is the best MRI marker of malignancy for atypical cirrhotic nodules: hypointensity in hepatobiliary phase alone or combined with other features? Classification after Gd-EOB-DTPA administration. J Magn Reson Imaging. 2012;36(3):648–57.

88. Ouedraogo W, Tran-Van Nhieu J, et al. Evaluation of noninvasive diagnostic criteria for hepatocellular carcinoma on pretransplant MRI (2010): correlation between MR imaging features and histological features on liver specimen. J Radiol. 2011;92(7–8):688–700.

89. Hwang J, Kim YK, Jeong WK, et al. Nonhypervascular Hypointense nodules at Gadoxetic acid-enhanced MR imaging in chronic liver disease: diffusion-weighted imaging for characterization. Radiology. 2015;276(1):137–46.

90. Kim JE, Kim SH, Lee SJ, Rhim H. Hypervascular hepatocellular carcinoma1 cm or smaller in patients with chronic liver disease: characterization with gadoxetic acid-enhanced MRI that includes diffusion-weighted imaging. AJR Am J Roentgenol. 2011;196(6):W758–65.

91. Petralia G, Summers PE, Agostini A, Ambrosini R, Cianci R, Cristel G, et al. Dynamic contrast-enhanced MRI in oncology: how we do it. Radiol Med. 2020;125(12):1288–300. https://doi.org/10.1007/s11547-020-01220-z Epub 2020 May 15. PMID: 32415476.

92. Granata V, Fusco R, Sansone M, Grassi R, Maio F, Palaia R, et al. Magnetic resonance imaging in the assessment of pancreatic cancer with quantitative parameter extraction by means of dynamic contrast-enhanced magnetic resonance imaging, diffusion kurtosis imaging and intravoxel incoherent motion diffusion-weighted imaging. Therap Adv Gastroenterol. 2020;13: 1756284819885052. https://doi.org/10.1177/1756284819885052 PMID: 32499833; PMCID: PMC7243396.

93. Zhang A, Song J, Ma Z, Chen T. Combined dynamic contrast-enhanced magnetic resonance imaging and diffusion-weighted imaging to predict neoadjuvant chemotherapy effect in FIGO stage IB2-IIA2 cervical cancers. Radiol Med. 2020;125(12):1233–42. https://doi.org/10.1007/s11547-020-01214-x Epub 2020 May 18. PMID: 32424659.

94. Petrillo A, Fusco R, Vallone P, Filice S, Granata V, Petrosino T, et al. Digital breast tomosynthesis and contrast-enhanced dual-energy digital mammography alone and in combination compared to 2D digital synthetized mammography and MR imaging in breast cancer detection and classification. Breast J. 2020;26(5):860–72. https://doi.org/10.1111/tbj.13739 Epub 2019 Dec 30. PMID: 31886607.

95. Sun NN, Ge XL, Liu XS, Xu LL. Histogram analysis of DCE-MRI for chemoradiotherapy response evaluation in locally advanced esophageal squamous cell carcinoma. Radiol Med. 2020;125(2):165–76. https://doi.org/10.1007/s11547-019-01081-1 Epub 2019 Oct 11. PMID: 31605354.

96. Minutoli F, Pergolizzi S, Blandino A, Mormina E, Amato E, Gaeta M. Effect of granulocyte colony-stimulating factor on bone marrow: evaluation by intravoxel incoherent motion and dynamic contrast-enhanced magnetic resonance imaging. Radiol Med. 2020;125(3):280–7. https://doi.org/10.1007/s11547-019-01115-8 Epub 2019 Dec 10. PMID: 31823293.

97. Fusco R, Sansone M, Granata V, Grimm R, Pace U, Delrio P, et al. Diffusion and perfusion MR parameters to assess preoperative short-course radiotherapy response in locally advanced rectal cancer: a comparative explorative study among standardized index of shape by DCE-MRI, intravoxel incoherent motion- and diffusion kurtosis imaging-derived parameters. Abdom Radiol (NY). 2019;44(11):3683–700. https://doi.org/10.1007/s00261-018-1801-z PMID: 30361867.

98. Lin CC, Cheng YF, Chiang HJ, et al. Pharmacokinetic analysis of dynamic contrast-enhanced magnetic resonance imaging for distinguishing

hepatocellular carcinoma from cholangiocarcinoma in pre-liver transplantation evaluation. Transplant Proc. 2016;48:1041–4.

99. Banerji A, Naish JH, Watson Y, et al. DCE- MRI model selection for investigating dis- ruption of microvascular function in livers with metastatic disease. J Magn Reson Imaging. 2012;35:196–203.

100. Liang H, Hu C, Lu J, Zhang T, Jiang J, Ding D, et al. Correlation of radiomic features on dynamic contrast-enhanced magnetic resonance with microvessel density in hepatocellular carcinoma based on different models. J Int Med Res. 2021;49(3):300060521997586. https://doi.org/10.1177/03 00060521997586 PMID: 33682491; PMCID: PMC7944531.

101. Sahani DV, Jiang T, Hayano K, Duda DG, Catalano OA, Ancukiewicz M, et al. Magnetic resonance imaging biomarkers in hepatocellular carcinoma: association with response and circulating biomarkers after sunitinib therapy. J Hematol Oncol. 2013;6:51. PMID: 23842041. https://doi.org/10.1186/1756-8722-6-51.

102. Khalifa F, Soliman A, El-Baz A, Abou El-Ghar M, El-Diasty T, Gimel'farb G, et al. Models and methods for analyzing DCE-MRI: a review. Med Phys. 2014;41:124301. PMID: 25471985. https://doi.org/10.1118/1.4898202.

103. Yang JF, Zhao ZH, Zhang Y, Zhao L, Yang LM, Zhang MM, et al. Dual-input two-compartment pharmacokinetic model of dynamic contrast-enhanced magnetic resonance imaging in hepatocellular carcinoma. World J Gastroenterol. 2016;22(13):3652–62. https://doi.org/10.3748/wjg.v22.i13.3652 PMID: 27053857; PMCID: PMC4814651.

104. Albano D, Stecco A, Micci G, Sconfienza LM, Colagrande S, Reginelli A, et al. Whole-body magnetic resonance imaging (WB-MRI) in oncology: an Italian survey. Radiol Med. 2021;126(2):299–305. https://doi.org/10.1007/s11547-02 0-01242-7 Epub 2020 Jun 22. PMID: 32572763.

105. Taverna C, Novelli L, De Renzis AGD, Calistri L, Tomei M, Occhipinti M, et al. The role of diffusion-weighted and dynamic contrast enhancement perfusion-weighted imaging in the evaluation of salivary glands neoplasms. Radiol Med. 2020;125(9):851–63. https://doi.org/10.1007/s11547-020-01182-2 Epub 2020 Apr 7. PMID: 32266692.

106. Lian S, Zhang C, Chi J, Huang Y, Shi F, Xie C. Differentiation between nasopharyngeal carcinoma and lymphoma at the primary site using whole-tumor histogram analysis of apparent diffusion coefficient maps. Radiol Med. 2020;125(7):647–53. https://doi.org/10.1007/s11547-020-01152-8 Epub 2020 Feb 18. PMID: 32072391.

107. Lan H, Lin G, Zhong W. A meta-analysis of the added value of diffusion weighted imaging in combination with contrast-enhanced magnetic resonance imaging for the diagnosis of small hepatocellular carcinoma lesser or equal to 2 cm. Oncol Lett. 2020;20(3):2739–48. https://doi.org/10.3 892/ol.2020.11805 Epub 2020 Jul 3. PMID: 32782590; PMCID: PMC7400770.

108. Zhang Y, Zhu Y, Zhang K, Liu Y, Cui J, Tao J, et al. Invasive ductal breast cancer: preoperative predict Ki-67 index based on radiomics of ADC maps. Radiol Med. 2020;125(2):109–16. https://doi.org/10.1007/s11547-019-01100-1 Epub 2019 Nov 6. PMID: 31696388.

109. Fornell-Perez R, Vivas-Escalona V, Aranda-Sanchez J, Gonzalez-Dominguez MC, Rubio-Garcia J, Aleman-Flores P, et al. Primary and post-chemoradiotherapy MRI detection of extramural venous invasion in rectal cancer: the role of diffusion-weighted imaging. Radiol Med. 2020;125(6):522–30. https://doi.org/10.1007/s11547-020-01137-7 Epub 2020 Feb 4. PMID: 32020526.

110. Messina C, Bignone R, Bruno A, Bruno A, Bruno F, Calandri M, et al. Diffusion-weighted imaging in oncology: an update. Cancers (Basel). 2020;12(6):1493. https://doi.org/10.3390/cancers12061493 PMID: 32521645; PMCID: PMC7352852.

111. Koh DM, Collins DJ. Diffusion-weighted MRI in the body: applications and challenges in oncology. AJR Am J Roentgenol. 2007;188(6):1622–35. https://doi.org/10.2214/AJR.06.1403 PMID: 17515386.

112. Barnes A, Alonzi R, Blackledge M, Charles-Edwards G, Collins DJ, Cook G, et al. UK quantitative WB-DWI technical workgroup: consensus meeting recommendations on optimisation, quality control, processing and analysis of quantitative whole-body diffusion-weighted imaging for cancer. Br J Radiol. 2018;91(1081):20170577. https://doi.org/10.1259/bjr.20170577 Epub 2017 Dec 7. PMID: 29076749; PMCID: PMC5966219.

113. Pandey P, Lewis H, Pandey A, Schmidt C, Dillhoff M, Kamel IR, et al. Updates in hepatic oncology imaging. Surg Oncol. 2017;26(2):195–206. https://doi.org/10.1016/j.suronc.2017.03.007 Epub 2017 Apr 6. PMID: 28577726.

114. Ogura A, Sotome H, Asai A, Fuju A. Evaluation of capillary blood volume in the lower limb muscles after exercise by intravoxel incoherent motion.

Radiol Med. 2020;125(5):474–80. https://doi.org/10.1007/s11547-020-01163-5 Epub 2020 Mar 12. PMID: 32166719.

115. Beyhan M, Sade R, Koc E, Adanur S, Kantarci M. The evaluation of prostate lesions with IVIM DWI and MR perfusion parameters at 3T MRI. Radiol Med. 2019;124(2):87–93. https://doi.org/10.1007/s11547-018-0930-3 Epub 2018 Oct 1. PMID: 30276599.

116. Dyvorne H, Jajamovich G, Kakite S, Kuehn B, Taouli B. Intravoxel incoherent motion diffusion imaging of the liver: optimal b-value subsampling and impact on parameter precision and reproducibility. Eur J Radiol. 2014;83(12):2109–13. https://doi.org/10.1016/j.ejrad.2014.09.003 Epub 2014 Sep 21. PMID: 25277521; PMCID: PMC4254063.

117. Granata V, Fusco R, Catalano O, Guarino B, Granata F, Tatangelo F, et al. Intravoxel incoherent motion (IVIM) in diffusion-weighted imaging (DWI) for Hepatocellular carcinoma: correlation with histologic grade. Oncotarget. 2016;7(48):79357–64. https://doi.org/10.18632/oncotarget.12689 PMID: 27764817; PMCID: PMC5346719.

118. Le Bihan D. What can we see with IVIM MRI? Neuroimage. 2019;187:56–67. https://doi.org/10.1016/j.neuroimage.2017.12.062 Epub 2017 Dec 22. PMID: 29277647.

119. Iima M. Perfusion-driven Intravoxel incoherent motion (IVIM) MRI in oncology: applications, challenges, and future trends. Magn Reson Med Sci. 2020. https://doi.org/10.2463/mrms.rev.2019-0124. Epub ahead of print.

120. Granata V, Fusco R, Catalano O, Filice S, Amato DM, Nasti G, et al. Early assessment of colorectal cancer patients with liver metastases treated with antiangiogenic drugs: the role of intravoxel incoherent motion in diffusion-weighted imaging. PLoS One. 2015;10(11):e0142876. https://doi.org/10.1371/journal.pone.0142876 PMID: 26566221; PMCID: PMC4643930.

121. Liang J, Li Z, Li J, Peng C, Dai W, He H, et al. Application of IVIM-DWI in detecting the tumor vasculogenic mimicry under antiangiogenesis combined with oxaliplatin treatment. Front Oncol. 2020;10:1376. https://doi.org/10.3389/fonc.2020.01376 PMID: 32974136; PMCID: PMC7461873.

122. He R, Ding Y, Mohamed ASR, Ng SP, Ger RB, Elhalawani H, et al. Simultaneously spatial and temporal Higher-Order Total Variations for noise suppression and motion reduction in DCE and IVIM. Proc SPIE Int Soc Opt Eng. 2020;11313:113132K. https://doi.org/10.1117/12.2549625 Epub 2020 Mar 10. PMID: 32753776; PMCID: PMC7401327.

123. Jensen JH, Helpern JA. MRI quantification of non-Gaussian water diffusion by kurtosis analysis. NMR Biomed. 2010;23(7):698–710. https://doi.org/10.1002/nbm.1518 PMID: 20632416; PMCID: PMC2997680.

124. Rosenkrantz AB, Padhani AR, Chenevert TL, Koh DM, De Keyzer F, Taouli B, et al. Body diffusion kurtosis imaging: basic principles, applications, and considerations for clinical practice. J Magn Reson Imaging. 2015;42(5):1190–202. https://doi.org/10.1002/jmri.24985 Epub 2015 Jun 26. PMID: 26119267.

125. Granata V, Fusco R, Reginelli A, Delrio P, Selvaggi F, Grassi R, et al. Diffusion kurtosis imaging in patients with locally advanced rectal cancer: current status and future perspectives. J Int Med Res. 2019;47(6):2351–60. https://doi.org/10.1177/0300060519827168 Epub 2019 Apr 28. PMID: 31032670; PMCID: PMC6567719.

126. Vidiri A, Minosse S, Piludu F, Pellini R, Cristalli G, Kayal R, et al. Cervical lymphadenopathy: can the histogram analysis of apparent diffusion coefficient help to differentiate between lymphoma and squamous cell carcinoma in patients with unknown clinical primary tumor? Radiol Med. 2019;124(1):19–26. https://doi.org/10.1007/s11547-018-0940-1 Epub 2018 Sep 8. PMID: 30196522.

127. Wu G, Zhao Z, Yao Q, Kong W, Xu J, Zhang J, et al. The study of clear cell renal cell carcinoma with MR diffusion Kurtosis tensor imaging and its Histopathologic correlation. Acad Radiol. 2018;25(4):430–8. https://doi.org/10.1016/j.acra.2017.10.016 Epub 2017 Nov 29. PMID: 29198944.

128. Wu B, Jia F, Li X, Zhang M, Han D, Jia Z. Amide proton transfer imaging vs diffusion kurtosis imaging for predicting histological grade of hepatocellular carcinoma. J Hepatocell Carcinoma. 2020;7:159–68. https://doi.org/10.2147/JHC.S272535 PMID: 33117750; PMCID: PMC7555354.

129. Wang GZ, Guo LF, Gao GH, Li Y, Wang XZ, Yuan ZG. Magnetic resonance diffusion kurtosis imaging versus diffusion-weighted imaging in evaluating the pathological grade of hepatocellular carcinoma. Cancer Manag Res. 2020;12:5147–58. https://doi.org/10.2147/CMAR.S254371 PMID: 32636677; PMCID: PMC7334009.

130. Yuan ZG, Wang ZY, Xia MY, Li FZ, Li Y, Shen Z, et al. Diffusion Kurtosis Imaging for Assessing the Therapeutic Response of Transcatheter Arterial Chemoembolization in Hepatocellular Carcinoma. J Cancer. 2020;11(8):2339–47. https://doi.org/10.7150/jca.32491 PMID: 32127960; PMCID: PMC7052943.

131. Guo R, Yang SH, Lu F, Han ZH, Yan X, Fu CX, et al. Evaluation of intratumoral heterogeneity by using diffusion kurtosis imaging and stretched exponential diffusion-weighted imaging in an orthotopic hepatocellular carcinoma xenograft model. Quant Imaging Med Surg. 2019;9(9):1566–78. https://doi.org/10.21037/qims.2019.08.18 PMID: 31667142; PMCID: PMC6785506.

132. Jia Y, Cai H, Wang M, Luo Y, Xu L, Dong Z, et al. Diffusion kurtosis MR imaging versus conventional diffusion-weighted imaging for distinguishing hepatocellular carcinoma from benign hepatic nodules. Contrast Media Mol Imaging. 2019;2019:2030147. https://doi.org/10.1155/2019/2030147 PMID: 31396023; PMCID: PMC6664697.

133. Lee MH, Kim SH, Park MJ, Park CK, Rhim H. Gadoxetic acid-enhanced hepatobiliary phase MRI and high-b-value diffusion-weighted imaging to distinguish well-differentiated hepatocellular carcinomas from benign nodules in patients with chronic liver disease. AJR Am J Roentgenol. 2011;197(5):W868–75. https://doi.org/10.2214/AJR.10.6237 PMID: 22021534.

134. Piana G, Trinquart L, Meskine N, Barrau V, Beers BV, Vilgrain V. New MR imaging criteria with a diffusion-weighted sequence for the diagnosis of hepatocellular carcinoma in chronic liver diseases. J Hepatol. 2011;55(1):126–32. https://doi.org/10.1016/j.jhep.2010.10.023 Epub 2010 Nov 23. PMID: 21145857.

135. McNamara MM, Thomas JV, Alexander LF, Little MD, Bolus DN, Li YE, et al. Diffusion-weighted MRI as a screening tool for hepatocellular carcinoma in cirrhotic livers: correlation with explant data-a pilot study. Abdom Radiol (NY). 2018;43(10):2686–92. https://doi.org/10.1007/s00261-018-1535-y PMID: 29500648.

136. Park MS, Kim S, Patel J, Hajdu CH, Do RK, Mannelli L, et al. Hepatocellular carcinoma: detection with diffusion-weighted versus contrast-enhanced magnetic resonance imaging in pretransplant patients. Hepatology. 2012;56(1):140–8. https://doi.org/10.1002/hep.25681 Epub 2012 Jun 18. PMID: 22370974.

137. Onur MR, Çiçekçi M, Kayalı A, Poyraz AK, Kocakoç E. The role of ADC measurement in differential diagnosis of focal hepatic lesions. Eur J Radiol. 2012;81(3):e171–6. https://doi.org/10.1016/j.ejrad.2011.01.116 Epub 2011 Feb 24. PMID: 21353418.

138. Kuai ZX, Sang XQ, Yao YF, Chu CY, Zhu YM. Evaluation of non-monoexponential diffusion models for hepatocellular carcinoma using b values up to 2000 s/mm^2: A short-term repeatability study. J Magn Reson Imaging. 2019;50(1):297–304. https://doi.org/10.1002/jmri.26563 Epub 2018 Nov 16. PMID: 30447032.

139. Rosenkrantz AB, Sigmund EE, Winnick A, Niver BE, Spieler B, Morgan GR, et al. Assessment of hepatocellular carcinoma using apparent diffusion coefficient and diffusion kurtosis indices: preliminary experience in fresh liver explants. Magn Reson Imaging. 2012;30(10):1534–40. https://doi.org/10.1016/j.mri.2012.04.020 Epub 2012 Jul 20. PMID: 22819175.

140. Goshima S, Kanematsu M, Noda Y, Kondo H, Watanabe H, Bae KT. Diffusion kurtosis imaging to assess response to treatment in hypervascular hepatocellular carcinoma. AJR Am J Roentgenol. 2015;204(5):W543–9. https://doi.org/10.2214/AJR.14.13235 PMID: 25905960.

141. Yilmaz C, Karaca CA, Iakobadze Z, Farajov R, Kilic K, Doganay L, et al. Factors affecting recurrence and survival after liver transplantation for hepatocellular carcinoma. Transplant Proc. 2018;50(10):3571–6. https://doi.org/10.1016/j.transproceed.2018.05.027 Epub 2018 May 29. PMID: 30577240.

142. Poon RT, Fan ST, Lo CM, Liu CL, Wong J. Long-term survival and pattern of recurrence after resection of small hepatocellular carcinoma in patients with preserved liver function: implications for a strategy of salvage transplantation. Ann Surg. 2002;235(3):373–82. https://doi.org/10.1097/00000658-200203000-00009 PMID: 11882759; PMCID: PMC1422443.

143. Pawlik TM, Delman KA, Vauthey JN, Nagorney DM, Ng IO, Ikai I, et al. Tumor size predicts vascular invasion and histologic grade: implications for selection of surgical treatment for hepatocellular carcinoma. Liver Transpl. 2005;11(9):1086–92. https://doi.org/10.1002/lt.20472 PMID: 16123959.

144. Nakanishi M, Chuma M, Hige S, Omatsu T, Yokoo H, Nakanishi K, et al. Relationship between diffusion-weighted magnetic resonance imaging and histological tumor grading of hepatocellular carcinoma. Ann Surg Oncol. 2012;19(4):1302–9. https://doi.org/10.1245/s10434-011-2066-8 Epub 2011 Sep 17. PMID: 21927976.

145. Chen J, Wu M, Liu R, Li S, Gao R, Song B. Preoperative evaluation of the histological grade of hepatocellular carcinoma with diffusion-weighted imaging: a meta-analysis. PLoS One. 2015;10(2):e0117661. https://doi.org/10.1371/journal.pone.0117661 PMID: 25658359; PMCID: PMC4320049.

146. Fusco R, Granata V, Pariante P, Cerciello V, Siani C, Di Bonito M, et al. Blood oxygenation level dependent magnetic resonance imaging and diffusion weighted MRI imaging for benign and malignant breast cancer discrimination. Magn Reson Imaging. 2021;75:51–9. https://doi.org/10.1016/j.mri.2020.10.008 Epub 2020 Oct 17. PMID: 33080334.

147. Patterson AJ, Priest AN, Bowden DJ, Wallace TE, Patterson I, Graves MJ, et al. Quantitative BOLD imaging at 3T: Temporal changes in hepatocellular carcinoma and fibrosis following oxygen challenge. J Magn Reson Imaging. 2016;44(3):739–44. https://doi.org/10.1002/jmri.25189 Epub 2016 Feb 19. PMID: 26892734; PMCID: PMC5042181.

148. Yuan F, Song B, Huang Z, Liu X, Xia C. Glucose as a stimulation agent in the BOLD functional magnetic resonance imaging for liver cirrhosis and hepatocellular carcinoma: a feasibility study. Abdom Radiol (NY). 2018;43(3):607–12. https://doi.org/10.1007/s00261-017-1264-7 PMID: 28730273.

149. Li B, Xu A, Huang Y, Peng L, Xiang K, Li Q, et al. Oxygen-challenge blood oxygen level-dependent magnetic resonance imaging for evaluation of early change of hepatocellular carcinoma to chemoembolization: a feasibility study. Acad Radiol. 2020;S1076–6332(20):30371–8. https://doi.org/10.1016/j.acra.2020.06.021 Epub ahead of print. PMID: 32747180.

150. Rhee TK, Larson AC, Prasad PV, et al. Feasibility of blood oxygenation level-dependent MR imaging to monitor hepatic transcatheter arterial embolization in rabbits. J Vasc Interv Radiol. 2005;16:1523–8. https://doi.org/10.1097/01.RVI.0000182179.87340.D7.

151. Choi JW, Kim H, Kim HC, et al. Blood oxygen level-dependent MRI for evaluation of early response of liver tumors to chemoembolization: an animal study. Anticancer Res. 2013;33:1887–92.

152. Benedetti G, Mori M, Panzeri MM, Barbera M, Palumbo D, Sini C, et al. CT-derived radiomic features to discriminate histologic characteristics of pancreatic neuroendocrine tumors. Radiol Med. 2021. https://doi.org/10.1007/s11547-021-01333-z. Epub ahead of print.

153. Agazzi GM, Ravanelli M, Roca E, Medicina D, Balzarini P, Pessina C, et al. CT texture analysis for prediction of EGFR mutational status and ALK rearrangement in patients with non-small cell lung cancer. Radiol Med. 2021. https://doi.org/10.1007/s11547-020-01323-7. Epub ahead of print.

154. Santone A, Brunese MC, Donnarumma F, Guerriero P, Mercaldo F, Reginelli A, et al. Radiomic features for prostate cancer grade detection through formal verification. Radiol Med. 2021;126(5):688–97. https://doi.org/10.1007/s11547-020-01314-8 Epub 2021 Jan 4. PMID: 33394366.

155. Cusumano D, Meijer G, Lenkowicz J, Chiloiro G, Boldrini L, Masciocchi C, et al. A field strength independent MR radiomics model to predict pathological complete response in locally advanced rectal cancer. Radiol Med. 2021;126(3):421–9. https://doi.org/10.1007/s11547-020-01266-z Epub 2020 Aug 24. PMID: 32833198; PMCID: PMC7937600.

156. Hu HT, Shan QY, Chen SL, Li B, Feng ST, Xu EJ, et al. CT-based radiomics for preoperative prediction of early recurrent hepatocellular carcinoma: technical reproducibility of acquisition and scanners. Radiol Med. 2020;125(8):697–705. https://doi.org/10.1007/s11547-020-01174-2 Epub 2020 Mar 21. PMID: 32200455.

157. Zhang L, Kang L, Li G, Zhang X, Ren J, Shi Z, et al. Computed tomography-based radiomics model for discriminating the risk stratification of gastrointestinal stromal tumors. Radiol Med. 2020;125(5):465–73. https://doi.org/10.1007/s11547-020-01138-6 Epub 2020 Feb 11. PMID: 32048155.

158. Gutmann DAP, Rospleszcz S, Rathmann W, Schlett CL, Peters A, Wachinger C, et al. MRI-derived radiomics features of hepatic fat predict metabolic states in individuals without cardiovascular disease. Acad Radiol. 2020;S1076–6332(20):30408–6. https://doi.org/10.1016/j.acra.2020.06.030 Epub ahead of print. PMID: 32800693.

159. Tomori Y, Yamashiro T, Tomita H, Tsubakimoto M, Ishigami K, Atsumi E, et al. CT radiomics analysis of lung cancers: differentiation of squamous cell carcinoma from adenocarcinoma, a correlative study with FDG uptake. Eur J Radiol. 2020;128:109032. https://doi.org/10.1016/j.ejrad.2020.109032 Epub 2020 Apr 26. PMID: 32361604.

160. Boldrini L, Cusumano D, Chiloiro G, Casà C, Masciocchi C, Lenkowicz J, et al. Delta radiomics for rectal cancer response prediction with hybrid 0.35 T magnetic resonance-guided radiotherapy (MRgRT): a hypothesis-generating study for an innovative personalized medicine approach. Radiol Med. 2019;124(2):145–53. https://doi.org/10.1007/s11547-018-0951-y Epub 2018 Oct 29. PMID: 30374650; PMCID: PMC6373341.

161. Fusco R, Granata V, Mazzei MA, Meglio ND, Roscio DD, Moroni C, et al. Quantitative imaging decision support (QIDS™) tool consistency evaluation and radiomic analysis by means of 594 metrics in lung carcinoma on chest

CT scan. Cancer Control. 2021;28:1073274820985786. https://doi.org/10.11 77/1073274820985786 PMID: 33567876.

162. Nardone V, Reginelli A, Guida C, Belfiore MP, Biondi M, Mormile M, et al. Delta-radiomics increases multicentre reproducibility: a phantom study. Med Oncol. 2020;37(5):38. https://doi.org/10.1007/s12032-020-01359-9 PMID: 32236847.

163. Paoletti M, Muzic SI, Marchetti F, Farina LM, Bastianello S, Pichiecchio A. Differential imaging of atypical demyelinating lesions of the central nervous system. Radiol Med. 2021. https://doi.org/10.1007/s11547-021-01334-y. Epub ahead of print.

164. Nazari M, Shiri I, Hajianfar G, Oveisi N, Abdollahi H, Deevband MR, et al. Noninvasive Fuhrman grading of clear cell renal cell carcinoma using computed tomography radiomic features and machine learning. Radiol Med. 2020;125(8):754–62. https://doi.org/10.1007/s11547-020-01169-z Epub 2020 Mar 19. PMID: 32193870.

165. Borhani AA, Catania R, Velichko YS, Hectors S, Taouli B, Lewis S. Radiomics of hepatocellular carcinoma: promising roles in patient selection, prediction, and assessment of treatment response. Abdom Radiol (NY). 2021. https:// doi.org/10.1007/s00261-021-03085-w. Epub ahead of print.

166. Sagir KA. Radiomics in hepatocellular carcinoma. J Gastrointest Cancer. 2020; 51(4):1165–8. https://doi.org/10.1007/s12029-020-00493-x PMID: 32844349.

167. Zhong X, Guan T, Tang D, Li J, Lu B, Cui S, et al. Differentiation of small (≤ 3 cm) hepatocellular carcinomas from benign nodules in cirrhotic liver: the added additive value of MRI-based radiomics analysis to LI-RADS version 2018 algorithm. BMC Gastroenterol. 2021;21(1):155. https://doi.org/10.1186/ s12876-021-01710-y PMID: 33827440; PMCID: PMC8028813.

168. Jiang H, Liu X, Chen J, Wei Y, Lee JM, Cao L, Wu Y, Duan T, Li X, Ma L, Song B. Man or machine? Prospective comparison of the version 2018 EASL, LI-RADS criteria and a radiomics model to diagnose hepatocellular carcinoma. Cancer Imaging. 2019;19(1). https://doi.org/10.1186/s40644-019-0266-9.

169. Mokrane FZ, Lu L, Vavasseur A, Otal P, Peron JM, Luk L, et al. Radiomics machine-learning signature for diagnosis of hepatocellular carcinoma in cirrhotic patients with indeterminate liver nodules. Eur Radiol. 2020;30(1): 558–70. https://doi.org/10.1007/s00330-019-06347-w Epub 2019 Aug 23. PMID: 31444598.

170. Houseni M, Mahmoud MA, Saad S, ElHussiny F, Shihab M. Advanced intra-tumoural structural characterisation of hepatocellular carcinoma utilising FDG-PET/CT: a comparative study of radiomics and metabolic features in 3D and 2D. Pol J Radiol. 2021;86:e64–73. https://doi.org/10.5114/pjr.2021.103239 PMID: 33708274; PMCID: PMC7934742.

171. Maruyama H, Yamaguchi T, Nagamatsu H, Shiina S. AI-based radiological imaging for HCC: current status and future of ultrasound. Diagnostics (Basel). 2021;11(2):292. https://doi.org/10.3390/diagnostics11020292 PMID: 33673229; PMCID: PMC7918339.

172. Yao Z, Dong Y, Wu G, Zhang Q, Yang D, Yu JH, et al. Preoperative diagnosis and prediction of hepatocellular carcinoma: Radiomics analysis based on multi-modal ultrasound images. BMC Cancer. 2018;18(1):1089. https://doi. org/10.1186/s12885-018-5003-4 PMID: 30419849; PMCID: PMC6233500.

173. Lai Q, Spoletini G, Mennini G, Laureiro ZL, Tsilimigras DI, Pawlik TM, et al. Prognostic role of artificial intelligence among patients with hepatocellular cancer: a systematic review. World J Gastroenterol. 2020;26(42):6679–88. https://doi.org/10.3748/wjg.v26.i42.6679 PMID: 33268955; PMCID: PMC7673961.

174. Chen Y, Liu Z, Mo Y, Li B, Zhou Q, Peng S, et al. Prediction of post-hepatectomy liver failure in patients with hepatocellular carcinoma based on radiomics using Gd-EOB-DTPA-enhanced MRI: the liver failure model. Front Oncol. 2021;11:605296. https://doi.org/10.3389/fonc.2021.605296 PMID: 33777748; PMCID: PMC7987905.

175. Zhang L, Hu J, Hou J, Jiang X, Guo L, Tian L. Radiomics-based model using gadoxetic acid disodium-enhanced MR images: associations with recurrence-free survival of patients with hepatocellular carcinoma treated by surgical resection. Abdom Radiol. 2021. https://doi.org/10.1007/s00261-021-03034-7. Epub ahead of print.

176. Kuang Y, Li R, Jia P, Ye W, Zhou R, Zhu R, et al. MRI-based Radiomics: Nomograms predicting the short-term response after transcatheter arterial chemoembolization (TACE) in hepatocellular carcinoma patients with diameter less than 5 cm. Abdom Radiol. 2021. https://doi.org/10.1007/s002 61-021-02992-2. Epub ahead of print.

177. Chen M, Cao J, Hu J, Topatana W, Li S, Juengpanich S, et al. Clinical-radiomic analysis for pretreatment prediction of objective response to first transarterial chemoembolization in hepatocellular carcinoma. Liver Cancer.

2021;10(1):38–51. https://doi.org/10.1159/000512028 Epub 2021 Jan 7. PMID: 33708638; PMCID: PMC7923935.

178. Jin Z, Chen L, Zhong B, Zhou H, Zhu H, Zhou H, et al. Machine-learning analysis of contrast-enhanced computed tomography radiomics predicts patients with hepatocellular carcinoma who are unsuitable for initial transarterial chemoembolization monotherapy: A multicenter study. Transl Oncol. 2021;14(4):101034. https://doi.org/10.1016/j.tranon.2021.101034 Epub 2021 Feb 7. PMID: 33567388; PMCID: PMC7873378.

179. Niu XK, He XF. Development of a computed tomography-based radiomics nomogram for prediction of transarterial chemoembolization refractoriness in hepatocellular carcinoma. World J Gastroenterol. 2021;27(2):189–207. https://doi.org/10.3748/wjg.v27.i2.189 PMID: 33510559; PMCID: PMC7807298.

180. Yuan G, Song Y, Li Q, Hu X, Zang M, Dai W, et al. Development and validation of a contrast-enhanced CT-based radiomics nomogram for prediction of therapeutic efficacy of anti-PD-1 antibodies in advanced HCC patients. Front Immunol. 2021;11:613946. https://doi.org/10.3389/fimmu.202 0.613946 PMID: 33488622; PMCID: PMC7820863.

181. Ma QP, He XL, Li K, Wang JF, Zeng QJ, Xu EJ, et al. Dynamic contrast-enhanced ultrasound Radiomics for hepatocellular carcinoma recurrence prediction after thermal ablation. Mol Imaging Biol. 2021. https://doi.org/1 0.1007/s11307-021-01578-0. Epub ahead of print.

182. Wu K, Shui Y, Sun W, Lin S, Pang H. Utility of radiomics for predicting patient survival in hepatocellular carcinoma with portal vein tumor thrombosis treated with stereotactic body radiotherapy. Front Oncol. 2020; 10:569435. https://doi.org/10.3389/fonc.2020.569435 PMID: 33178598; PMCID: PMC7594107.

183. Nie P, Yang G, Guo J, Chen J, Li X, Ji Q, et al. A CT-based radiomics nomogram for differentiation of focal nodular hyperplasia from hepatocellular carcinoma in the non-cirrhotic liver. Cancer Imaging. 2020;20:20.

184. Wu J, Liu A, Cui J, Chen A, Song Q, Xie L. Radiomics-based classification of hepatocellular carcinoma and hepatic hemangioma on precontrast magnetic resonance images. BMC Med Imaging. 2019;19:23.

185. Liang W, Shao J, Liu W, Ruan S, Tian W, Zhang X, et al. Differentiating hepatic Epithelioid Angiomyolipoma from hepatocellular carcinoma and focal nodular hyperplasia via Radiomics models. Front Oncol. 2020;10: 564307.

186. Cellina M, Pirovano M, Ciocca M, Gibelli D, Floridi C, Oliva G. Radiomic analysis of the optic nerve at the first episode of acute optic neuritis: an indicator of optic nerve pathology and a predictor of visual recovery? Radiol Med. 2021;126(5):698–706. https://doi.org/10.1007/s11547-020-01318-4 Epub 2021 Jan 3. PMID: 33392980.

187. Granata V, Fusco R, Venanzio Setola S, Sandomenico F, Luisa Barretta M, Belli A, et al. Major and ancillary features according to LI-RADS in the assessment of combined hepatocellular-cholangiocarcinoma. Radiol Oncol. 2020;54(2):149–58. https://doi.org/10.2478/raon-2020-0029 PMID: 32463393; PMCID: PMC7276649.

188. Granata V, Fusco R, Setola SV, Picone C, Vallone P, Belli A, et al. Microvascular invasion and grading in hepatocellular carcinoma: correlation with major and ancillary features according to LIRADS. Abdom Radiol (NY). 2019;44(8):2788–800. https://doi.org/10.1007/s00261-019-02056-6 PMID: 31089780.

189. Fowler KJ, Potretzke TA, Hope TA, Costa EA, Wilson SR. LI-RADS M (LR-M): definite or probable malignancy, not specific for hepatocellular carcinoma. Abdominal Radiol. 2018;43(1):149–57. https://doi.org/10.1007/s00261-017-11 96-2.

190. Chernyak V, Fowler KJ, Kamaya A, Kielar AZ, Elsayes KM, Bashir MR, et al. Liver imaging reporting and data system (LI-RADS) version 2018: imaging of hepatocellular carcinoma in at-risk patients. Radiology. 2018;289(3):816–30. https://doi.org/10.1148/radiol.2018181494.

191. Kamath A, Roudenko A, Hecht E, Sirlin C, Chernyak V, Fowler K, et al. CT/ MR LI-RADS 2018: clinical implications and management recommendations. Abdominal Radiol. 2019;44(4):1306–22. https://doi.org/10.1007/s00261-018-1 868-6.

192. Dietrich CF, Nolsoe CP, Barr RG, Berzigotti A, Burns PN, Cantisani V, et al. Guidelines and good clinical practice recommendations for contrast- enhanced ultrasound (CEUS) in the liver-update 2020 WFUMB in cooperation with EFSUMB, AFSUMB, AIUM, and FLAUS. Ultrasound Med Biol. 2020;46(10):2579–604. https://doi.org/10.1016/j.ultrasmedbio.2 020.04.030.

193. Jo PC, Jang HJ, Burns PN, Burak KW, Kim TK, Wilson SR. Integration of contrast-enhanced US into a multimodality approach to imaging of nodules

Granata *et al. Infectious Agents and Cancer*   (2021) 16:53

Page 22 of 22

in a cirrhotic liver: how I Do it. Radiology. 2017;282(2):317–31. https://doi.org/10.1148/radiol.2016151732.

194. Kielar AZ, Chernyak V, Bashir MR, Do RK, Fowler KJ, Mitchell DG, et al. LI-RADS 2017: An update. J Magn Reson Imaging JMRI. 2018;47(6):1459–74. https://doi.org/10.1002/jmri.26027.

195. An C, Lee CH, Byun JH, Lee MH, Jeong WK, Choi SH, et al. Intraindividual comparison between Gadoxetate-enhanced magnetic resonance imaging and dynamic computed tomography for characterizing focal hepatic lesions: a multicenter, multireader study. Korean J Radiol. 2019;20(12):1616–26. https://doi.org/10.3348/kjr.2019.0363.

196. Kim YY, Kim MJ, Kim EH, Roh YH, An C. Hepatocellular carcinoma versus other hepatic malignancy in cirrhosis: performance of LI-RADS version 2018. Radiology. 2019;291(1):72–80. https://doi.org/10.1148/radiol.2019181995.

197. Zheng W, Li Q, Zou XB, Wang JW, Han F, Li F, et al. Evaluation of contrast-enhanced US LI-RADS version 2017: application on 2020 liver nodules in patients with hepatitis B infection. Radiology. 2020;294(2):299–307. https://doi.org/10.1148/radiol.2019190878.

198. Marrero JA, Kulik LM, Sirlin CB, Zhu AX, Finn RS, Abecassis MM, et al. Diagnosis, staging, and Management of Hepatocellular Carcinoma: 2018 practice guidance by the American Association for the Study of Liver Diseases. Hepatology. 2018;68(2):723–50. https://doi.org/10.1002/hep.29913.

199. Granata V, Grassi R, Fusco R, Setola SV, Palaia R, Belli A, et al. Assessment of ablation therapy in pancreatic cancer: the radiologist's challenge. Front Oncol. 2020;10:560952. https://doi.org/10.3389/fonc.2020.560952 PMID: 33330028; PMCID: PMC7731725.

200. Park EK, Kim HJ, Kim CY, et al. A comparison between surgical resection and radiofrequency ablation in the treatment of hepatocellular carci- Noma. Ann Surg Treat Res. 2014;87:72–80.

201. Kim GA, Shim JH, Kim MJ, et al. Radio- frequency ablation as an alternative to hepatic resection for single small hepatocellular carcino- mas. Br J Surg. 2016;103:126–35.

202. Liu PH, Hsu CY, Hsia CY, et al. Surgical re- section versus radiofrequency ablation for single hepatocellular carcinoma ≤ 2 cm in a propensity score model. Ann Surg. 2016;263:538–45.

203. Wang JH, Wang CC, Hung CH, et al. Survival comparison between surgical resection and radiofrequency ablation for patients in BCLC very early/early stage hepatocellular carcinoma. J Hepatol. 2012;56:412–8.

204. Gory I, Fink M, Bell S, et al. Melbourne liver group. Radiofrequency ablation versus re- section for the treatment of early stage hepato- cellular carcinoma: a multicenter Australian study. Scand J Gastroenterol. 2015;50:567–76.

205. Gavriilidis P, Askari A, Azoulay D. Survival following redo hepatectomy vs radiofrequency ablation for recurrent hepatocellular carcinoma: a systematic review and meta-analysis. HPB (Oxford). 2017;19:3–9.

206. Knavel EM, Brace CL. Tumor ablation: com- Mon modalities and general practices. Tech Vasc Interv Radiol. 2013;16:192–200.

207. Brace CL. Radiofrequency and microwave ablation of the liver, lung, kidney, and bone: what are the differences? Curr Probl Diagn Radiol. 2009;38:135–43.

208. Revel-Mouroz P, Otal P, Jaffro M, et al. Other non-surgical treatments for liver cancer. Rep Pract Oncol Radiother. 2017;22:181–92.

209. Sainani NI, Gervais DA, Mueller PR, Arellano RS. Imaging after percutaneous radiofrequency ablation of hepatic tumors: part 1, normal findings. AJR Am J Roentgenol. 2013;200(1):184–93. https://doi.org/10.2214/AJR.12.8478 PMID: 23255761.

210. Yuan H, Liu F, Li X, Guan Y, Wang M. Transcatheter arterial chemoembolization combined with simultaneous DynaCT-guided radiofrequency ablation in the treatment of solitary large hepatocellular carcinoma. Radiol Med. 2019;124(1):1–7. https://doi.org/10.1007/s11547-018-0932-1 Epub 2018 Aug 21. PMID: 30132184; PMCID: PMC6339665.

211. Catalano O, Izzo F, Vallone P, Sandomenico F, Albino V, Nunziata A, et al. Integrating contrast-enhanced sonography in the follow-up algorithm of hepatocellular carcinoma treated with radiofrequency ablation: single cancer center experience. Acta Radiol. 2015;56(2):133–42. https://doi.org/10.1177/0284185114521108 Epub 2014 Feb 12. PMID: 24523360.

212. Sugimoto K, Moriyasu F, Saito K, Kobayashi Y, Itoi T. Multimodality imaging to assess immediate response following irreversible electroporation in patients with malignant hepatic tumors. J Med Ultrason (2001). 2017;44(3):247–54. https://doi.org/10.1007/s10396-016-0767-0 Epub 2016 Dec 8. PMID: 27933441.

213. Sugimoto K, Moriyasu F, Kobayashi Y, et al. Irreversible electroporation for nonthermal tumor ablation in patients with hepatocellular carcinoma: initial clinical experience in Japan. Jpn J Radiol. 2015;33:424–32.

214. Granata V, Fusco R, Catalano O, Piccirillo M, De Bellis M, Izzo F, et al. Percutaneous ablation therapy of hepatocellular carcinoma with irreversible electroporation: MRI findings. AJR Am J Roentgenol. 2015;204(5):1000–7. https://doi.org/10.2214/AJR.14.12509 PMID: 25905934.

215. Gasljevic G, Edhemovic I, Cemazar M, Brecelj E, Gadzijev EM, Music MM, et al. Histopathological findings in colorectal liver metastases after electrochemotherapy. PLoS One. 2017;12:e0180709. https://doi.org/10.1371/journal.pone.0180709.

216. Boc N, Edhemovic I, Kos B, Music MM, Brecelj E, Trotovsek B, et al. Ultrasonographic changes in the liver tumors as indicators of adequate tumor coverage with electric field for effective electrochemotherapy. Radiol Oncol. 2018;52(4):383–91. https://doi.org/10.2478/raon-2018-0041 PMID: 30352044; PMCID: PMC6287182.

217. Tarantino L, Busto G, Nasto A, Fristachi R, Cacace L, Talamo M, et al. Percutaneous electrochemotherapy in the treatment of portal vein tumor thrombosis at hepatic hilum in patients with hepatocellular carcinoma in cirrhosis: a feasibility study. World J Gastroenterol. 2017;23(5):906–18. https://doi.org/10.3748/wjg.v23.i5.906 PMID: 28223736; PMCID: PMC5296208.

218. Granata V, Grassi R, Fusco R, Setola SV, Belli A, Piccirillo M, et al. Abbreviated MRI protocol for the assessment of ablated area in HCC patients. Int J Environ Res Public Health. 2021;18(7):3598. https://doi.org/10.3390/ijerph18073598 PMID: 33808466; PMCID: PMC8037601.

219. Lencioni R, Llovet JM. Modified RECIST (mRECIST) assessment for hepatocellular carcinoma. Semin Liver Dis. 2010;30(1):52–60. https://doi.org/10.1055/s-0030-1247132 Epub 2010 Feb 19. PMID: 20175033.

Publisher's Note